第四章 Plasmonics的前沿和应用

4.1 表面等离激元共振（SPR）及应用

各种纳米金属结构的SPR，SERS，光通讯，非线性现象，sensors等

4.2 表面等离激元（SPP）波导

槽形波导，杂化波导，介质金属混合波导，纳米金属球链波导，柱形波导等

4.3 周期性结构中SPP性质

色散关系，几何共振，超透射等

古英 ygu@pku.edu.cn 2010年4月

4.1 表面等离激元共振（SPR）及应用

各种形状金属颗粒SPR的共振范围

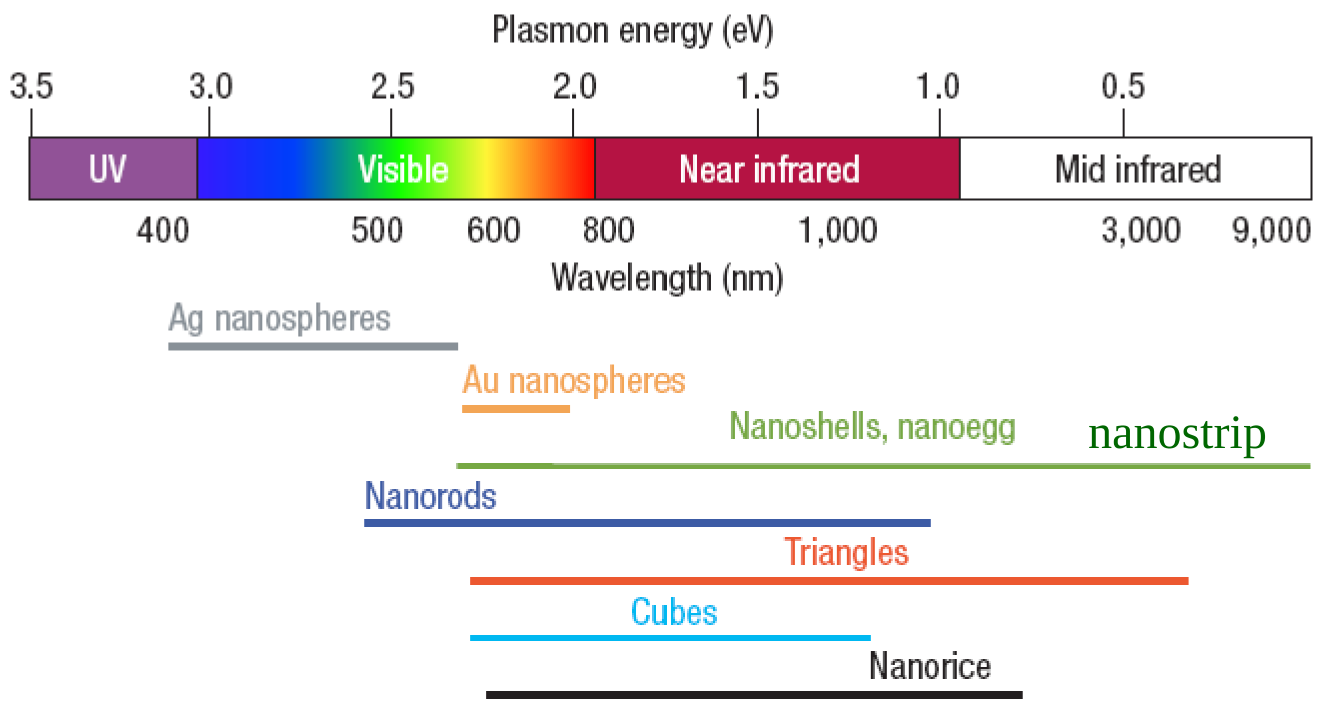

结论：通过调节纳米金属颗粒的形状，SPR可发生在可见光、红外和中红外波段。

实际上：在太赫兹和微波波段，SPR的研究也很广泛。

Nano-optics from sensing to waveguiding, N.J. Halas, nature photonics | VOL 1 |641| 2007

金小球的SPR及SERS

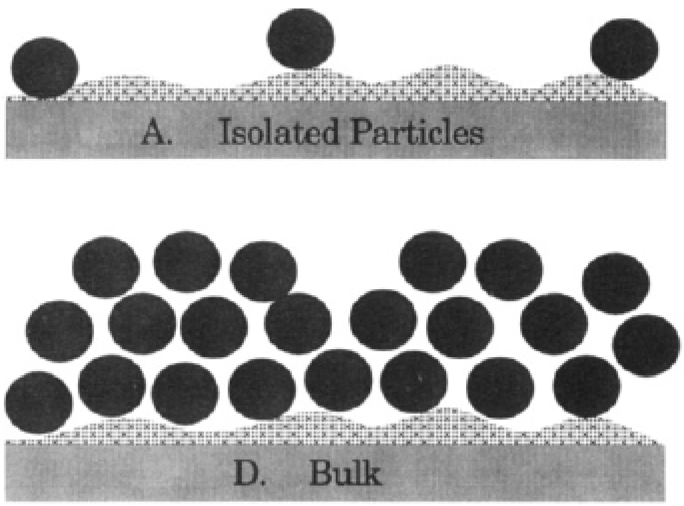

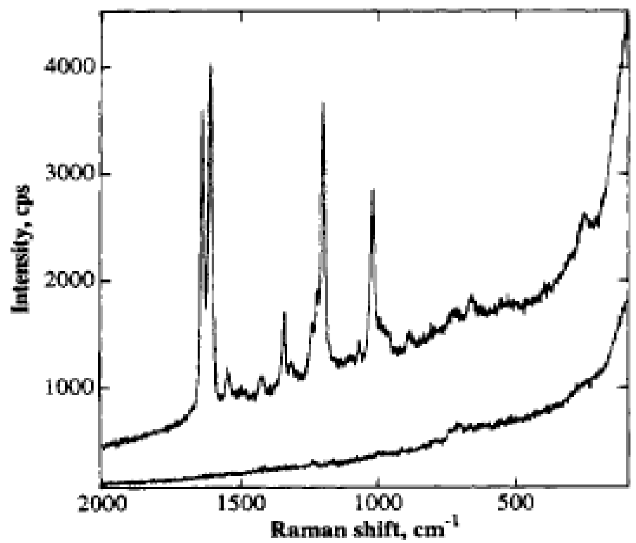

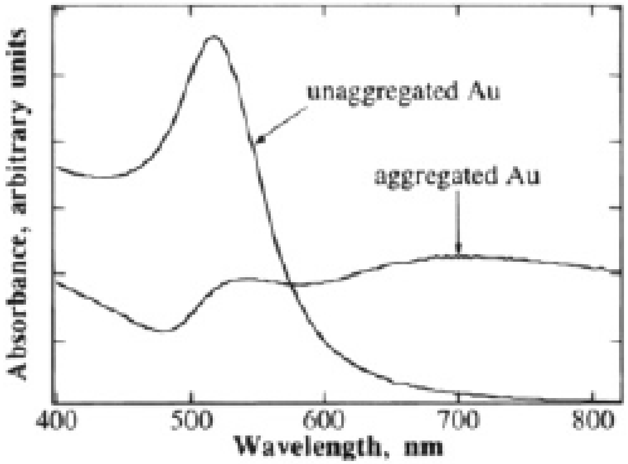

结果：13nm的金小球，在isolated情况下，共振在520nm，在聚集时，共振在700nm。以及在647nm共振时的SERS。

Preparation and Characterization of Au colloids Monolayers

Katherine C. Grabar et al, Anal. Chem. 1995,67, 735-743

银纳米岛的SPR及SERS

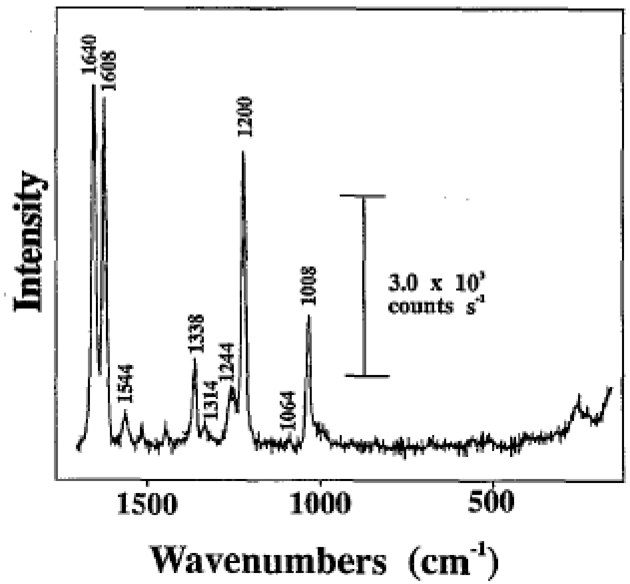

FIG. 10. SER spectrum of 1.0 monolayer of BPE spin coated on a Ag island film, d_m=8 nm. 10 mW of λ_{ex}=722 nm.

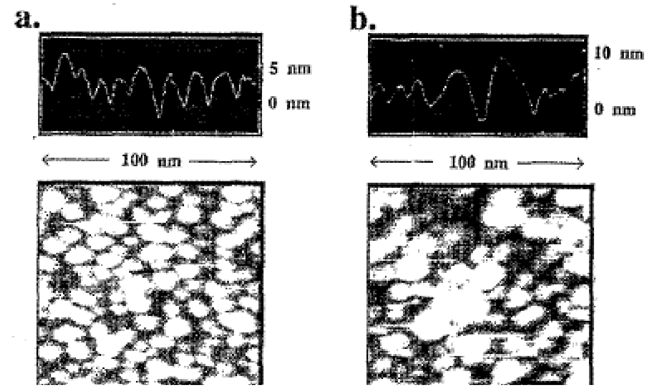

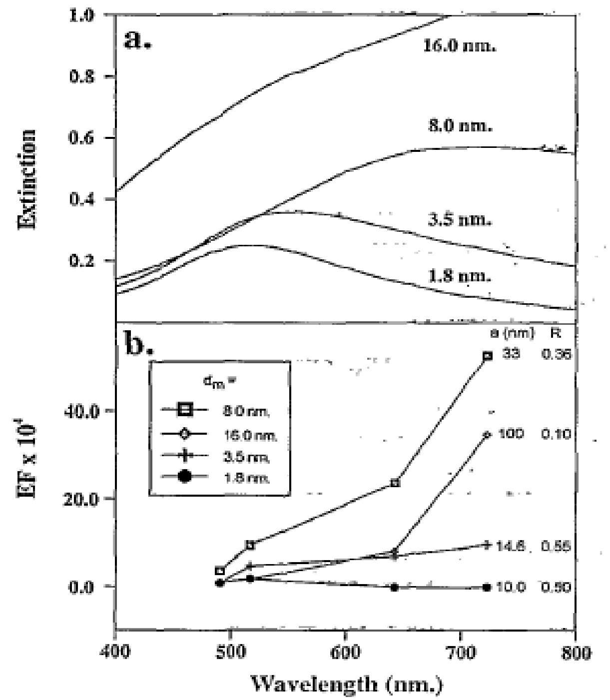

结果：随着纳米小球尺寸的增加，共振红移，场增益系数增加，以及在722nm共振时的SERS。

[Atomic force microscopy and surface-enhanced Raman spectroscopy. I. Ag island films and Ag film over polymer nanosphere surfaces supported on glass]

R. P. Van Duyne et al. J. Chern. Phys. 99 ,2101(1993).

银纳米三角形结构的制备及通讯波段SPR

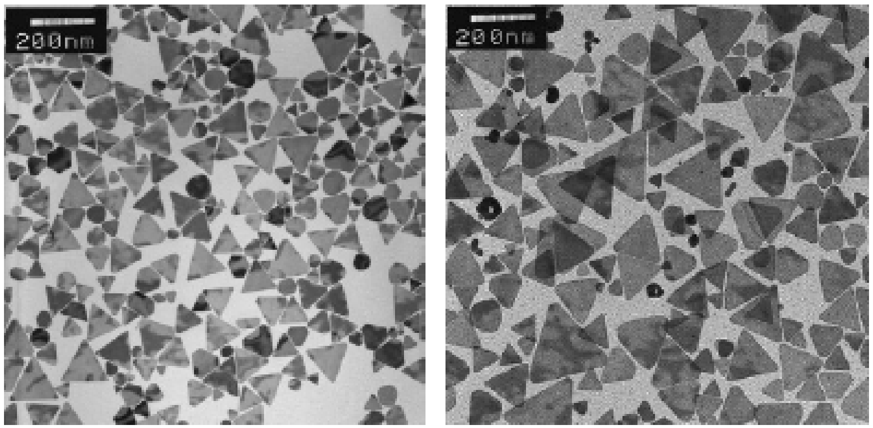

Figure 3. Representative TEM images of Ag nanoprisms prepared by illumination of Ag seeds with green (left) and red (red2, right) LEDs.

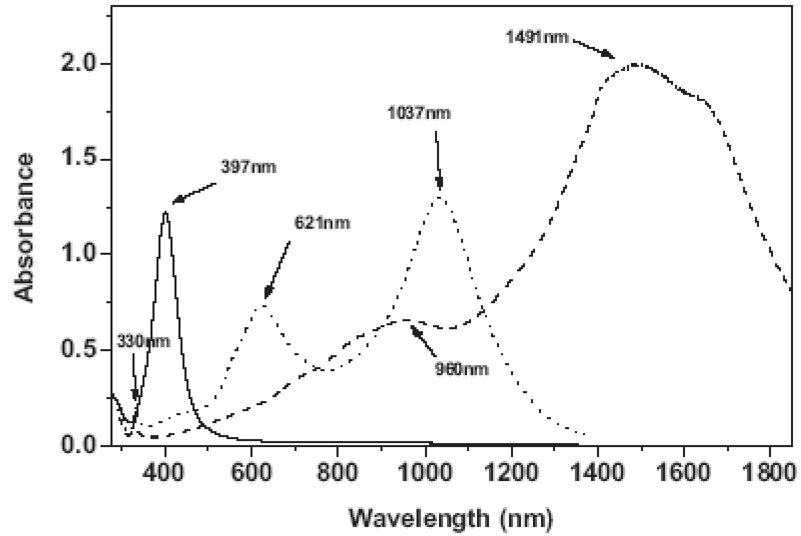

结果：除了光波段，我们看到了在1000到1500纳米间的SPR

[Formation of Silver Nanoprisms with Surface Plasmons at Communication Wavelengths]
Vytautas Bastys et al, Adv. Funct. Mater. 2006, 16, 766–773

银纳米三角形结构的SPR及近场分布

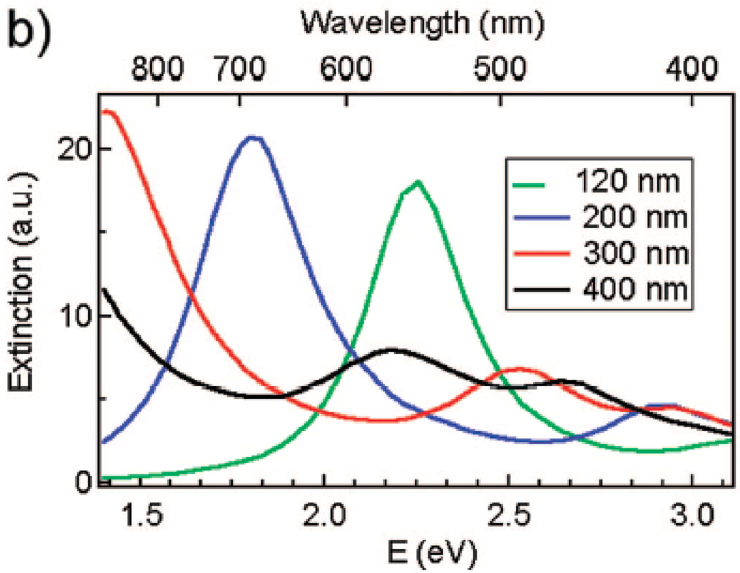

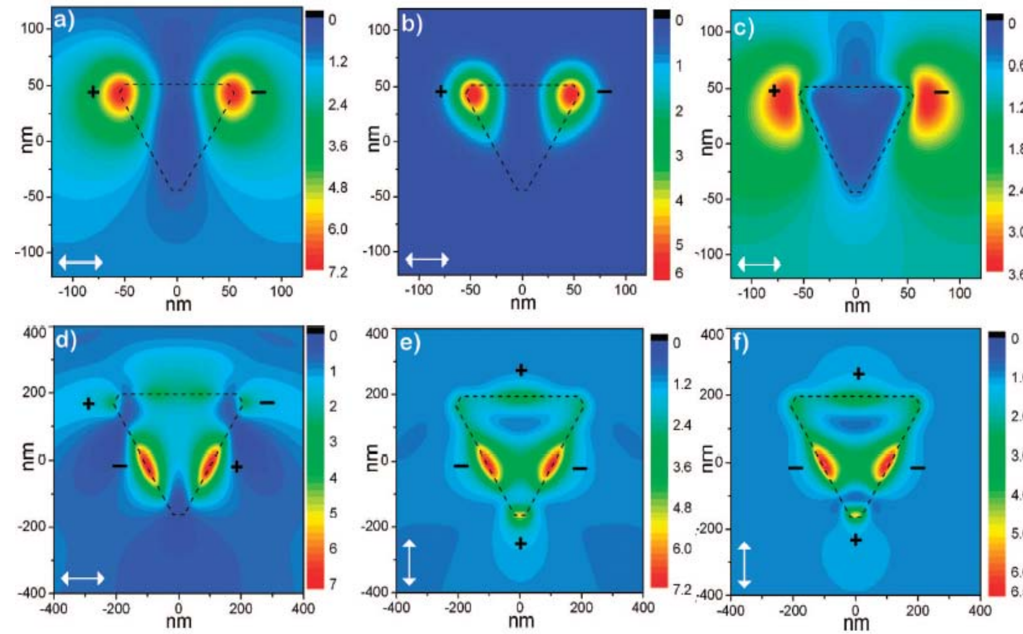

Figure 6. Calculated optical near-field distribution of the Ag nanoprism for 633 nm excitation. Top row: dipolar mode for nanoprism with

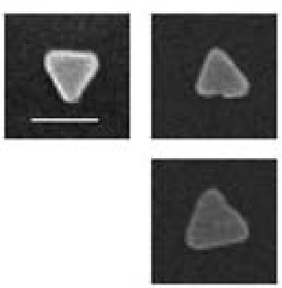

结果：随纳米三角形结构尺度的增加，共振红移；上图给出电偶极和电四极共振时的电场分布和电荷分布。

Optical Near-Field Mapping of Plasmonic Nanoprisms
Matthias Rang et al, NANO LETTERS (2008) Vol. 8, No. 10,3357-3363

SNOM近场分布

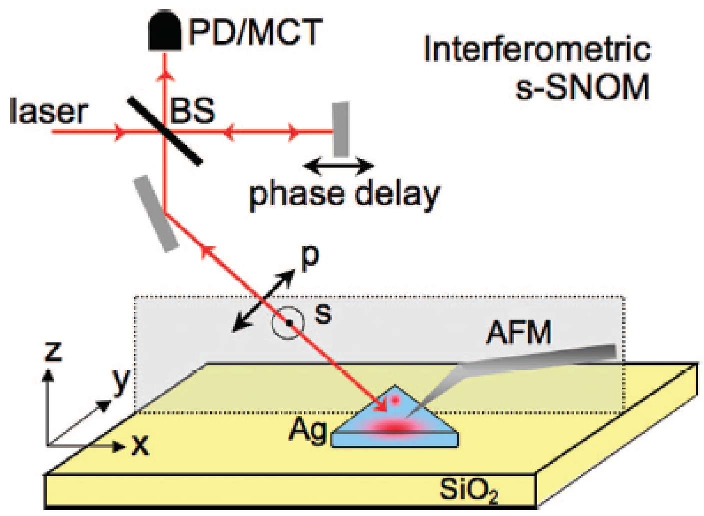

结果：用**SNOM**探测到的纳米三角形结构的形貌及共振时的近场分布，与理论计算相符。

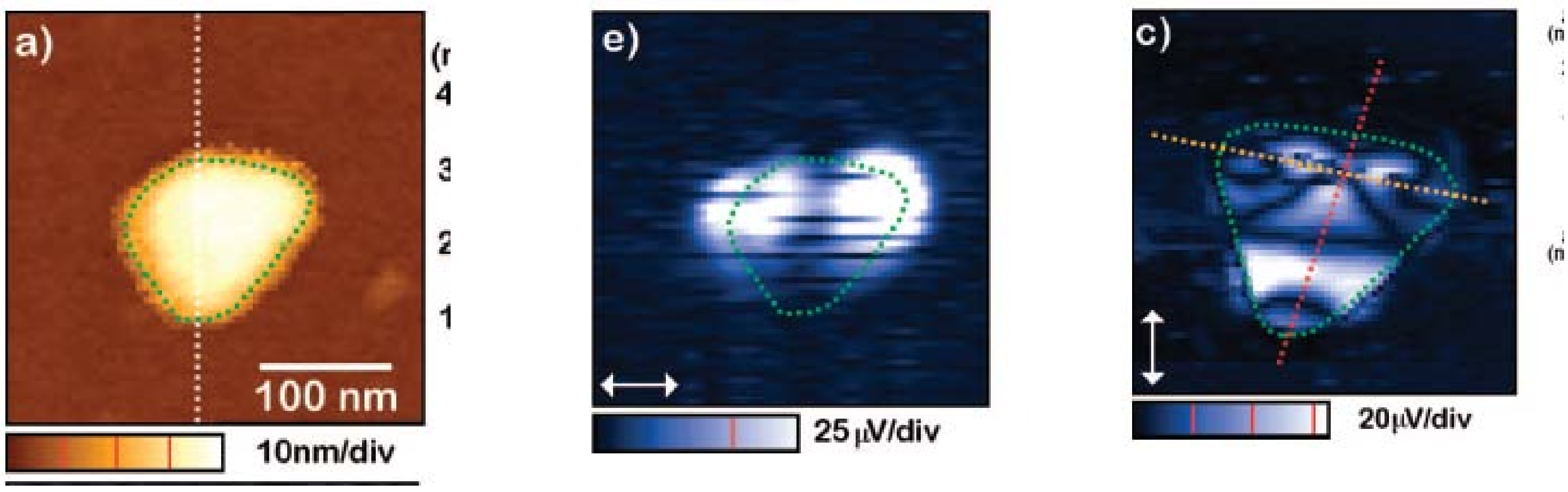

Optical Near-Field Mapping of Plasmonic Nanoprisms

Matthias Rang et al, NANO LETTERS (2008) Vol. 8, No. 10,3357-3363

银Nanobars 和 Nanorices 的SPR

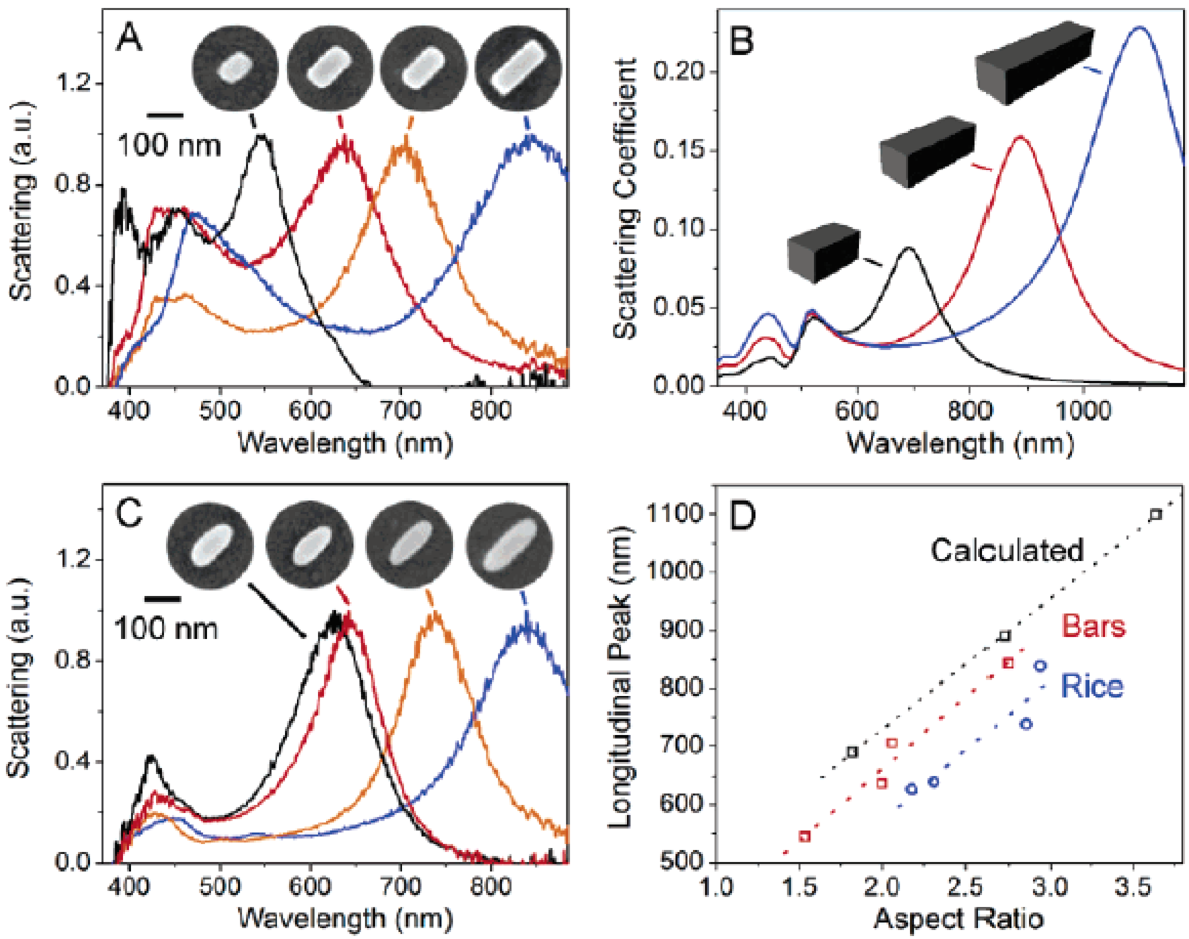

结果：制备出的银纳米颗粒尺度在百纳米内，共振在光波段，用散射谱表征**SPR**。理论计算用**DDA**。

Synthesis and Optical Properties of Silver Nanobars and Nanorice

Benjamin J. Wiley et al, NANO LETTERS (2007) Vol. 7, 1032。

金Nanorods 的SPR及SERS

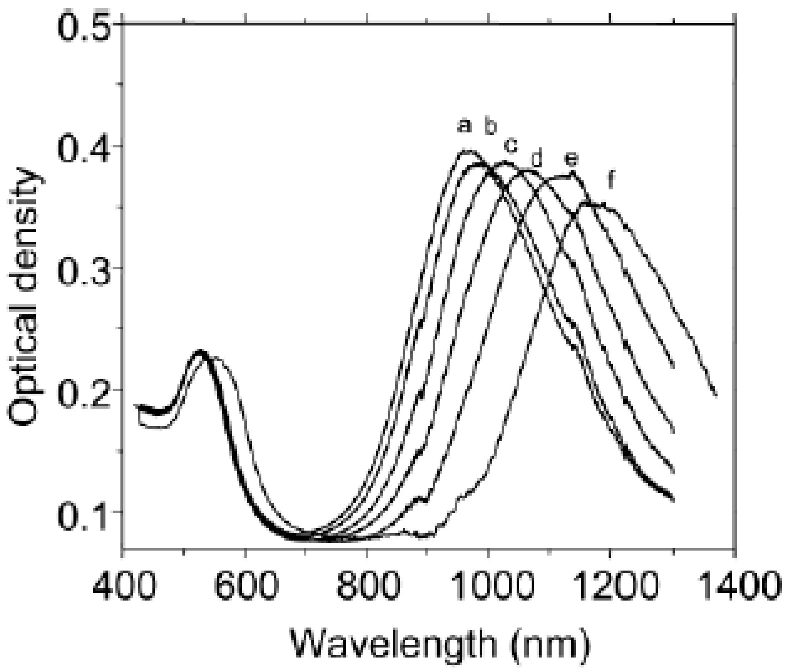

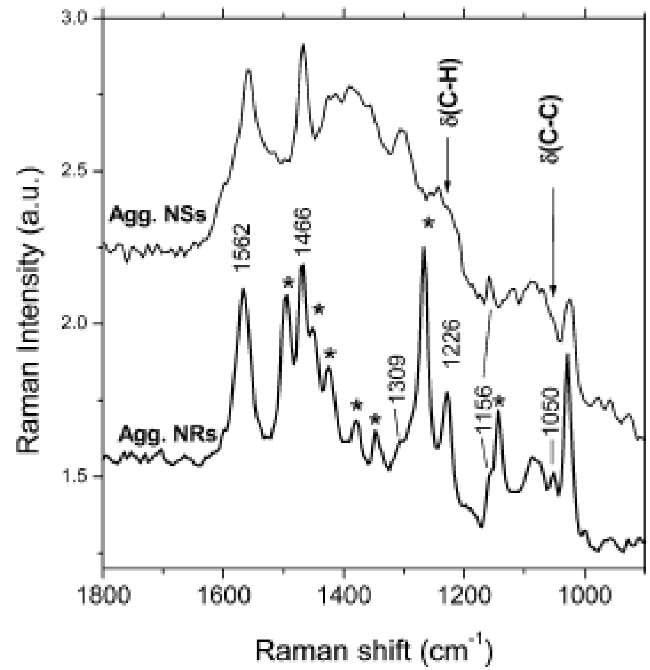

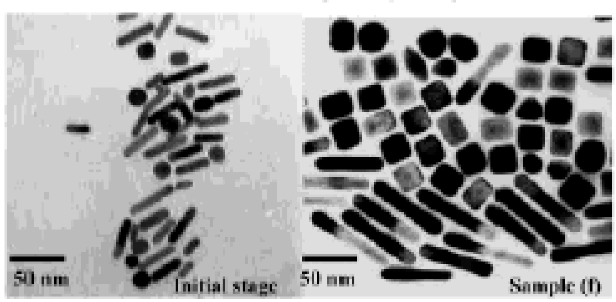

结果：制备出的金纳米颗粒尺度在百纳米的尺度，共振波长在光到近红外,可增强**SERS**。

Preparation and Growth Mechanism of Gold Nanorods (NRs) Using Seed-Mediated Growth Method
Babak Nikoobakht and Mostafa A. El-Sayed，Chem. Mater. 2003, 15, 1957-1962
Surface-Enhanced Raman Scattering Studies on Aggregated Gold Nanorod,
Babak Nikoobakht and Mostafa A. El-Sayed, J. Phys. Chem. A 2003, 107, 3372-3378

纳米金笼的SPR

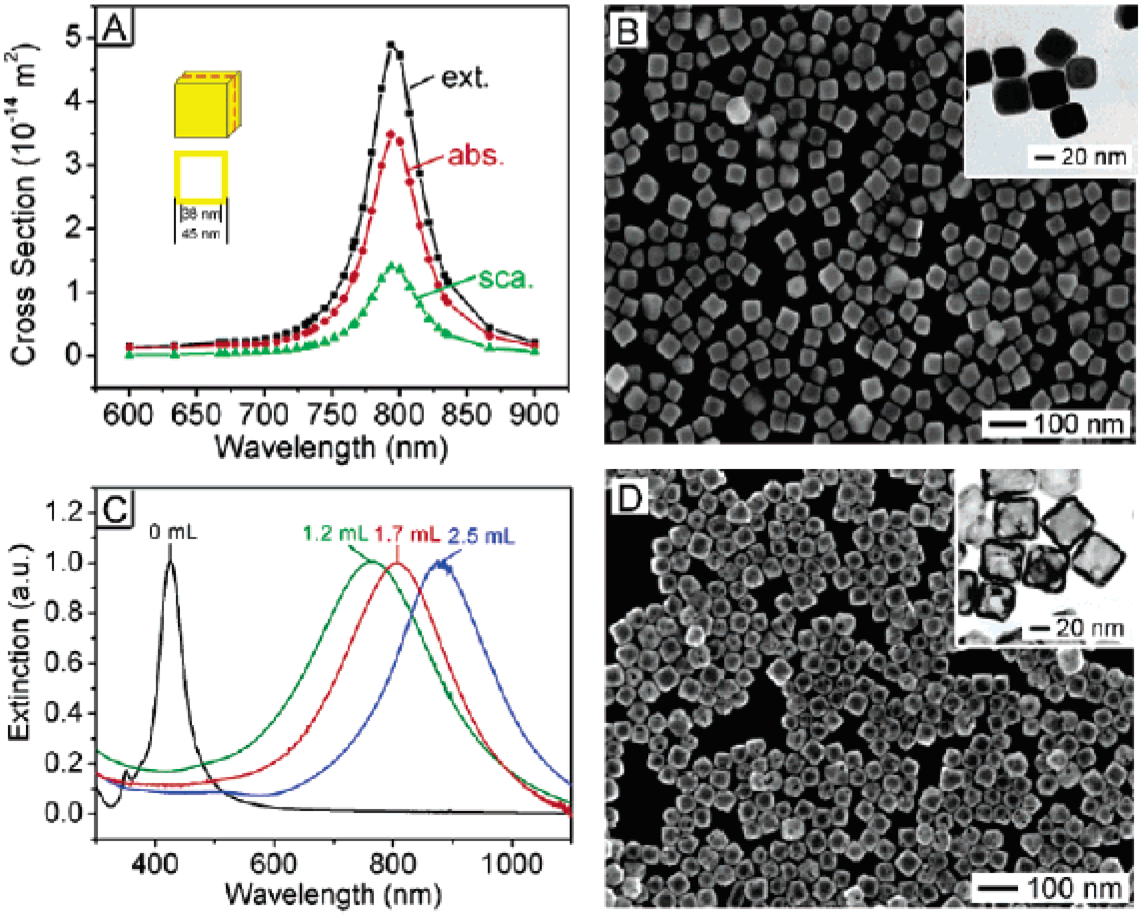

结果：制备出的纳米金笼尺度在百纳米内，共振波长在光波段，可用于癌症细胞的靶向治疗或免疫等。

Immuno Gold Nanocages with Tailored Optical Properties for Targeted Photothermal Destruction of Cancer Cells，Jingyi Chen et al, Nano letters, 7, 1318 (2007).

金Nanostar的SPR及SERS

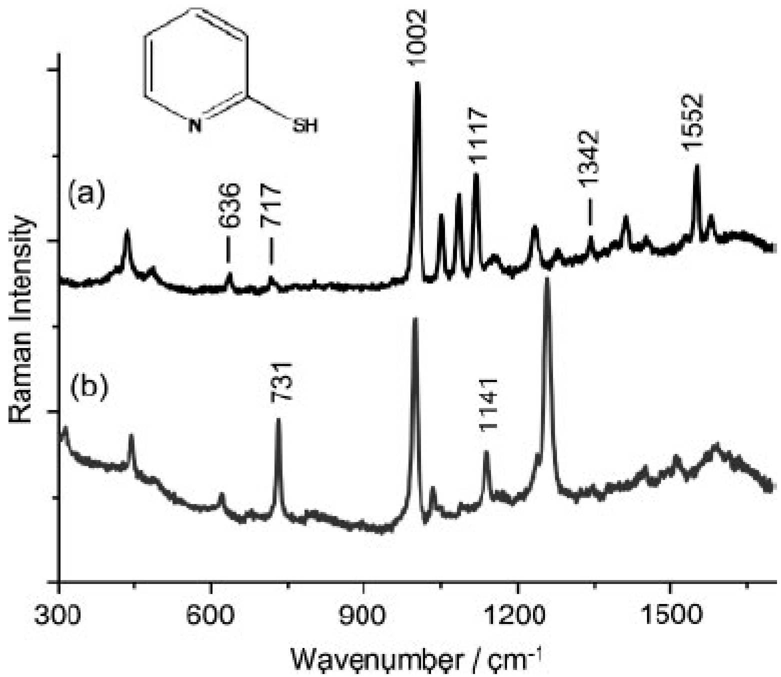

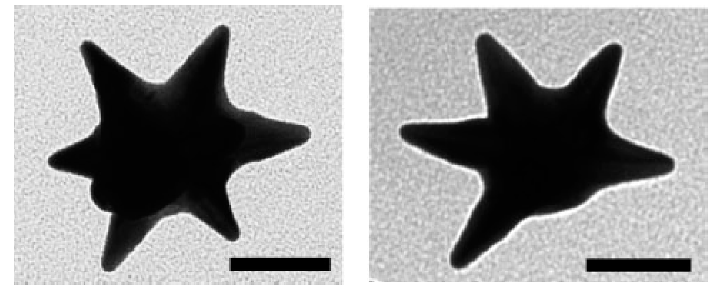

star-shaped gold nanoparticles. The scale bars are 50 nm.

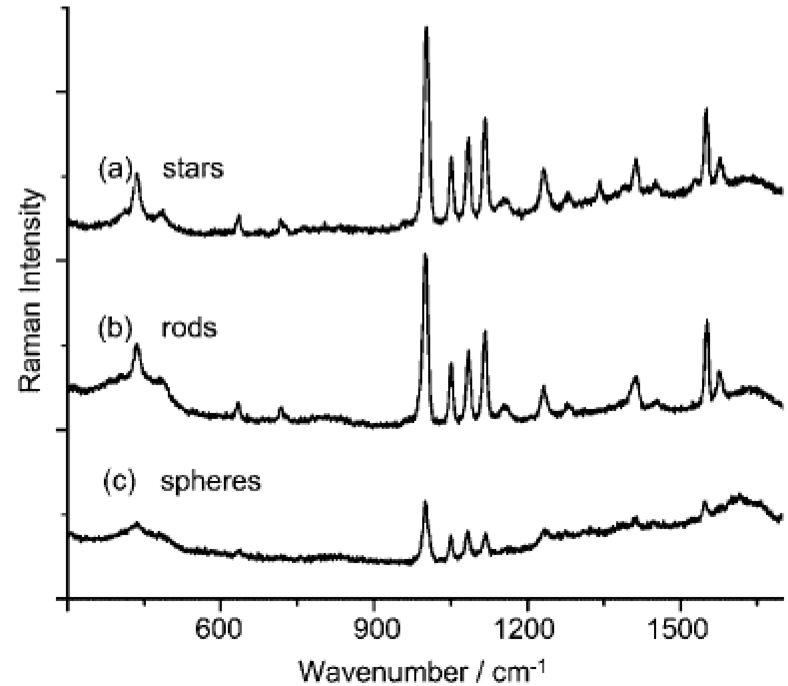

结果：制备出的纳米金星在增强表面拉曼散射方面的应用。一方面，出现更多拉曼峰，另一方面，强度增加。

Immuno Gold Nanocages with Tailored Optical Properties for Targeted Photothermal Destruction of Cancer Cells，Jingyi Chen et al, Nano letters, 7, 1318 (2007).

金Nanocrescent的SPR及SERS

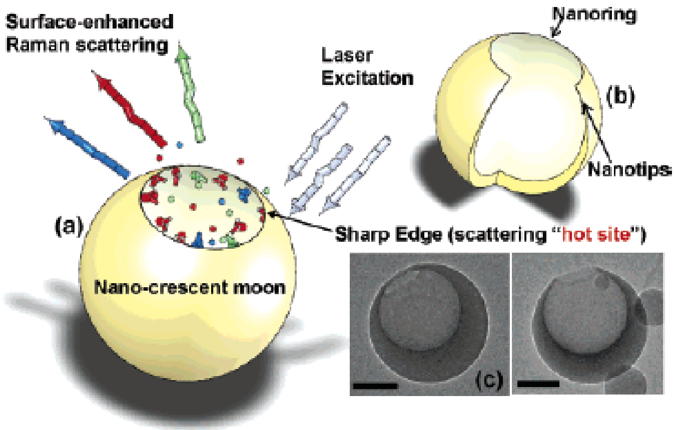

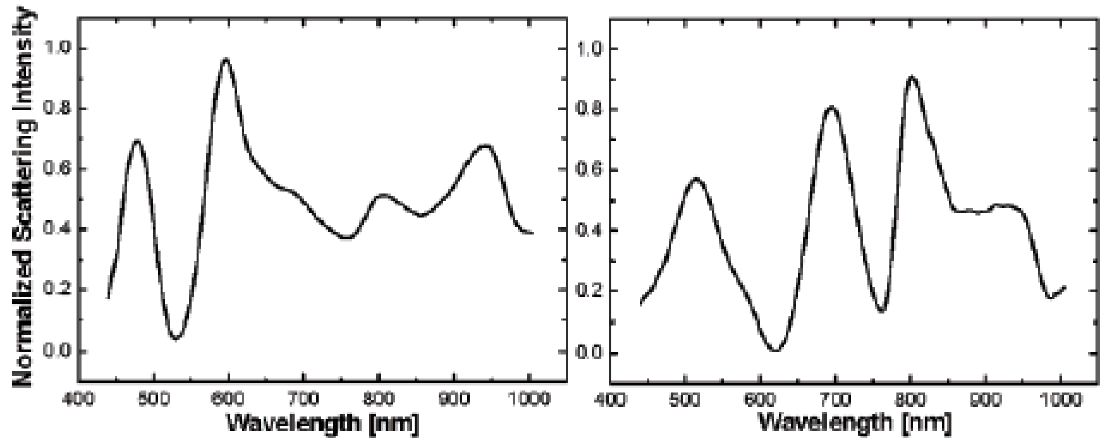

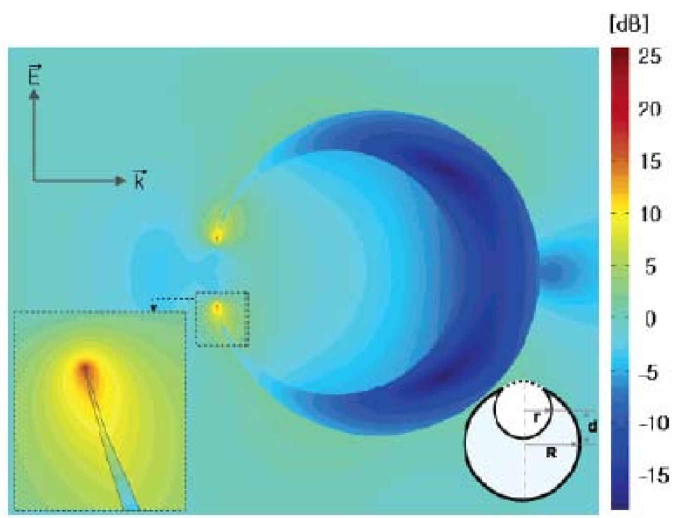

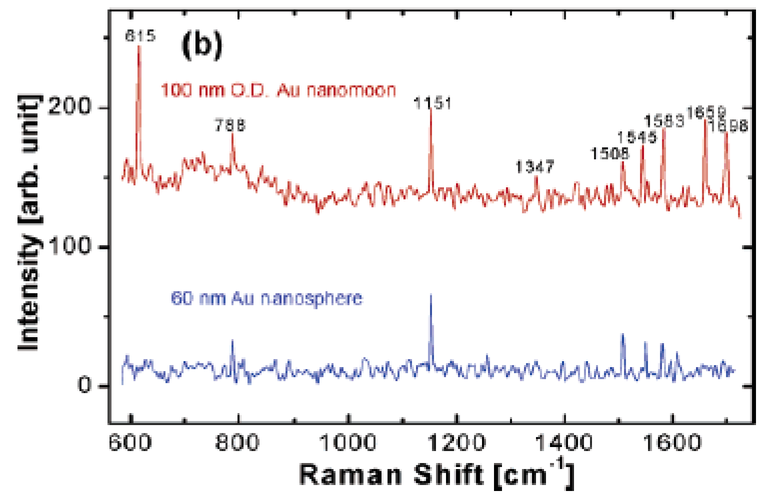

结果：制备出的纳米金月形，出现多重共振，电场局域在尖角，在增强表面拉曼散射方面的应用。

Nanophotonic Crescent Moon Structures with Sharp Edge for Ultrasensitive Biomolecular Detection by Local Electromagnetic Field Enhancement Effect, Y. Lu et al, Nano letters, 5, 119 (2005).

金Nanoring的多重SPR

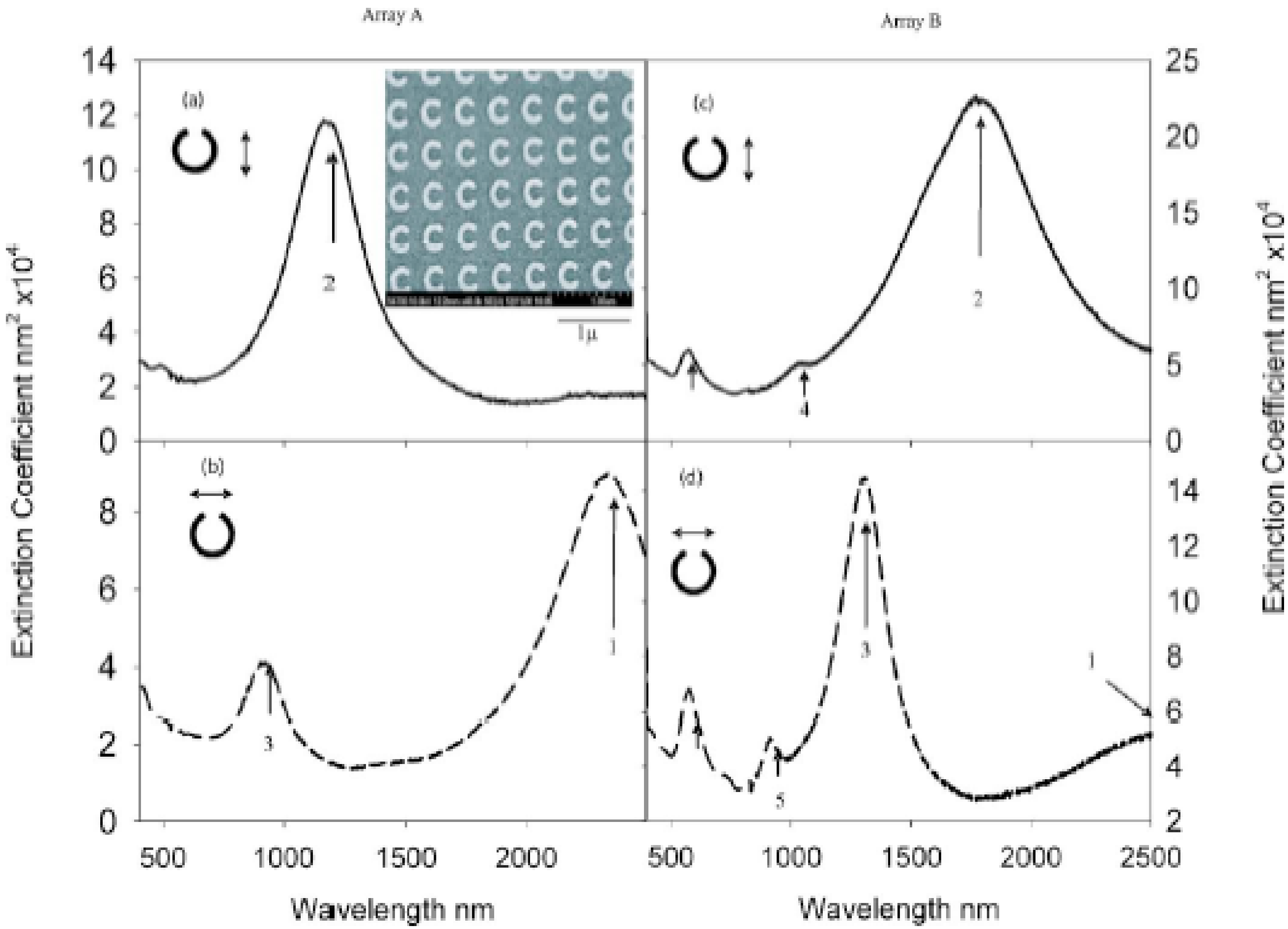

135nm radius **215nm radius**

结果：制备出的纳米C形，出现多重共振，1,2,3,4,5.

[Multiple plasmon resonances from gold nanostructures，]

A. K. Sheridan et al, APPLIED PHYSICS LETTERS 90, 143105 (2007).

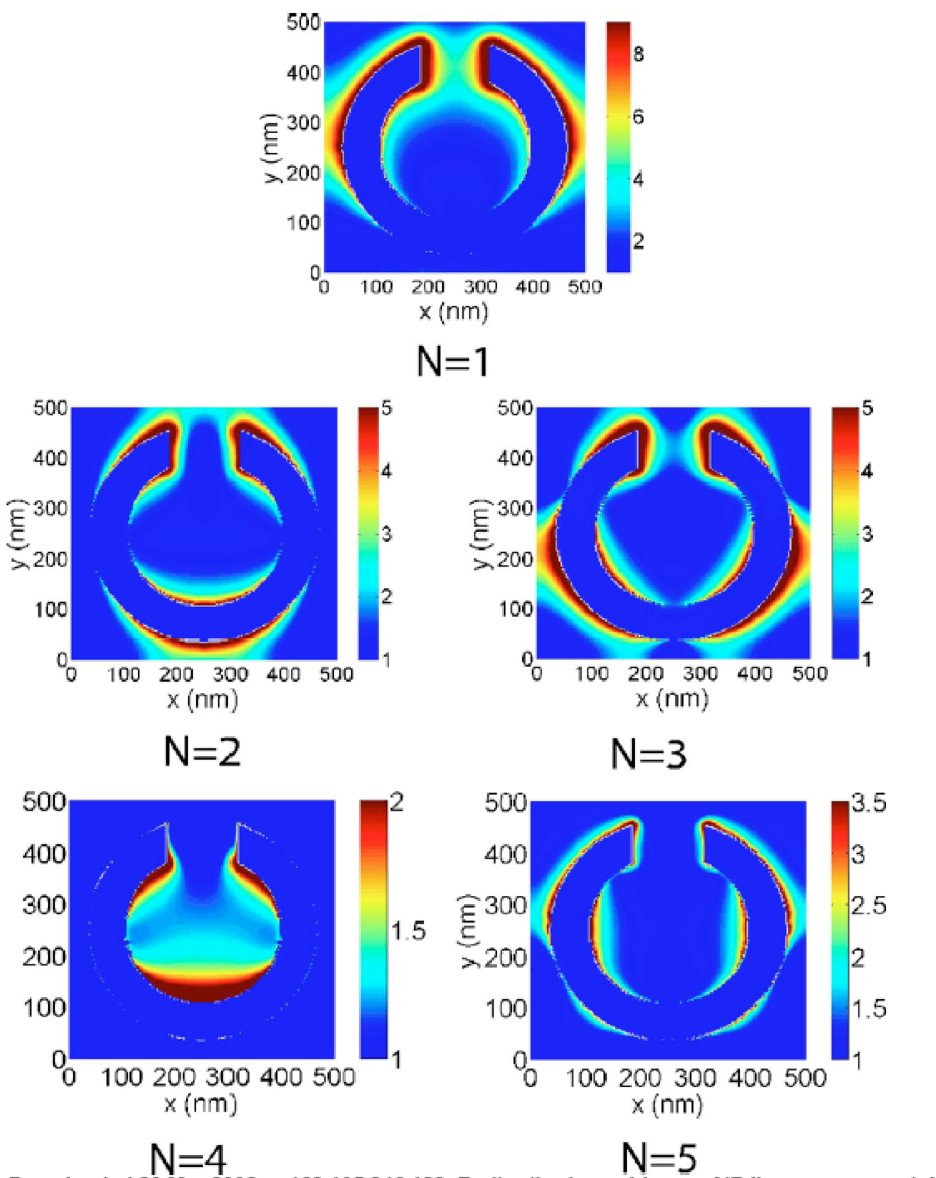

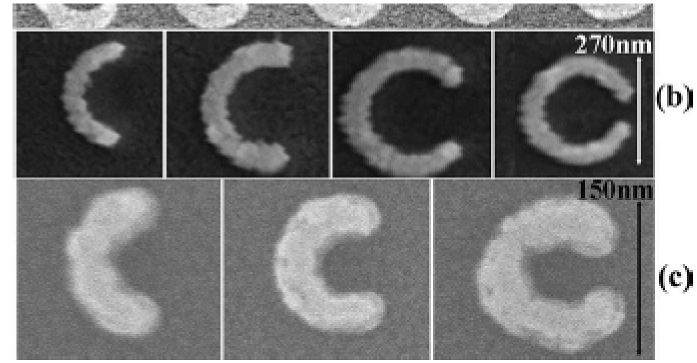

以上模式的电场分布。

[Multiple plasmon resonances from gold nanostructures，](#)

A. K. Sheridan et al, APPLIED PHYSICS LETTERS 90, 143105 (2007).

银纳米金属颗粒间的SPR相互作用

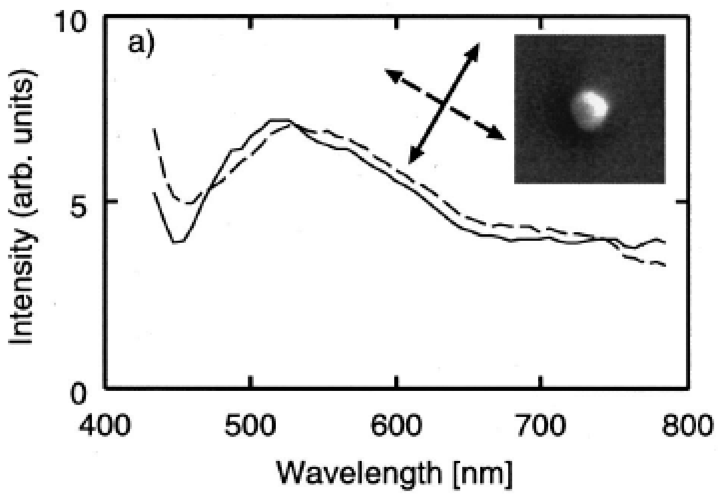

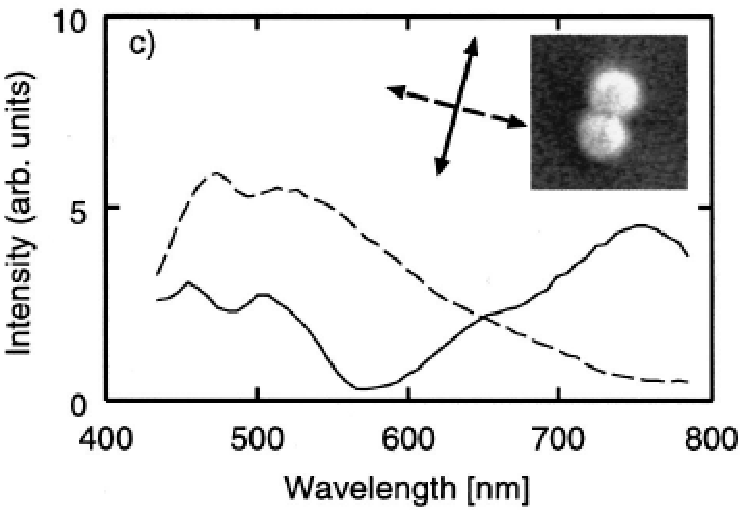

结果：**100nm**直径的银球共振在**520nm**左右，两个银球放在一起时，加平行中心线的光场，共振红移到**760nm**，加垂直光场时，共振蓝移到**470nm**。

Resonant light scattering from individual Ag nanoparticles and particle pairs
Hiroharu Tamarua，Appl. Phys. Lett., Vol. 80, 1827 (2002).

百纳米金棒间的SPR耦合

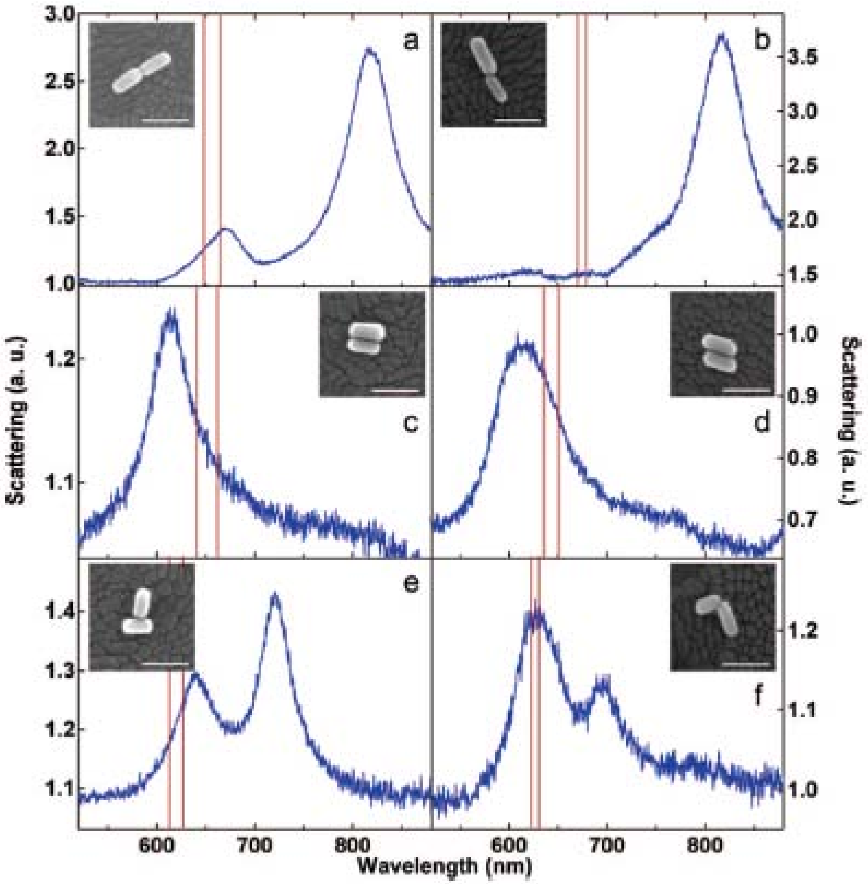

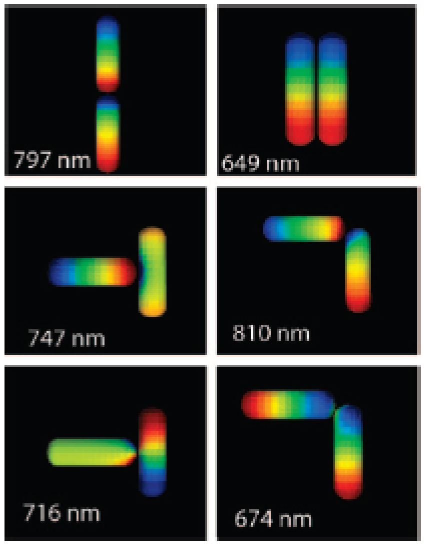

结果：金的结果与银类似，平行排列时**SPR**红移，垂直时蓝移，相互垂直是发生分裂。

Plasmon Coupling of Gold Nanorods at Short Distances and in Different Geometries

Alison M. Funston et al, NANO LETTERS (2009) Vol. 9, No. 4,1651-1658

SPR的“能级”分裂图

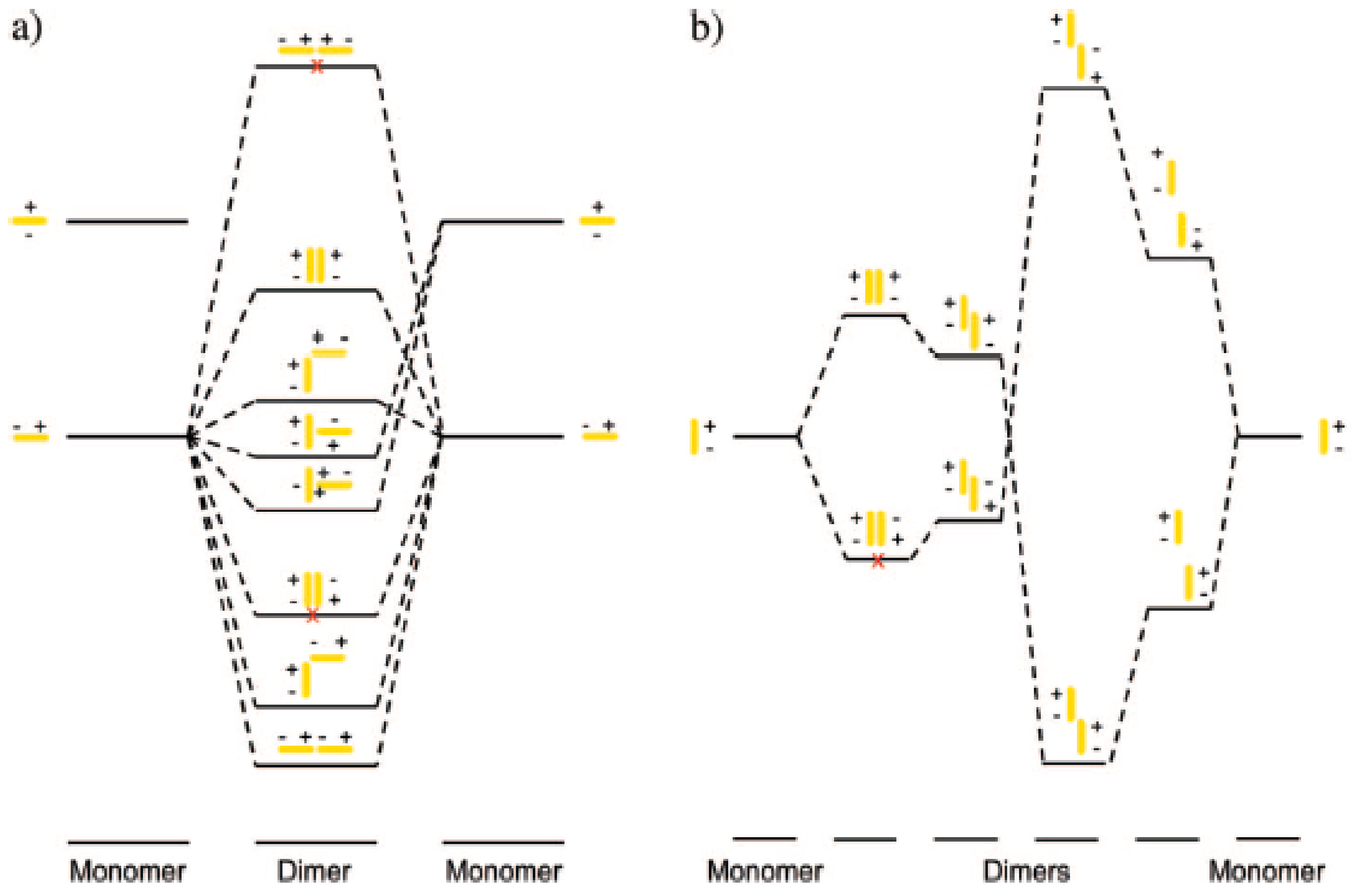

[Plasmon Coupling of Gold Nanorods at Short Distances and in Different Geometries]
Alison M. Funston et al, NANO LETTERS (2009) Vol. 9, No. 4,1651-1658

百纳米量级金棒SPR耦合与金棒间距离的关系

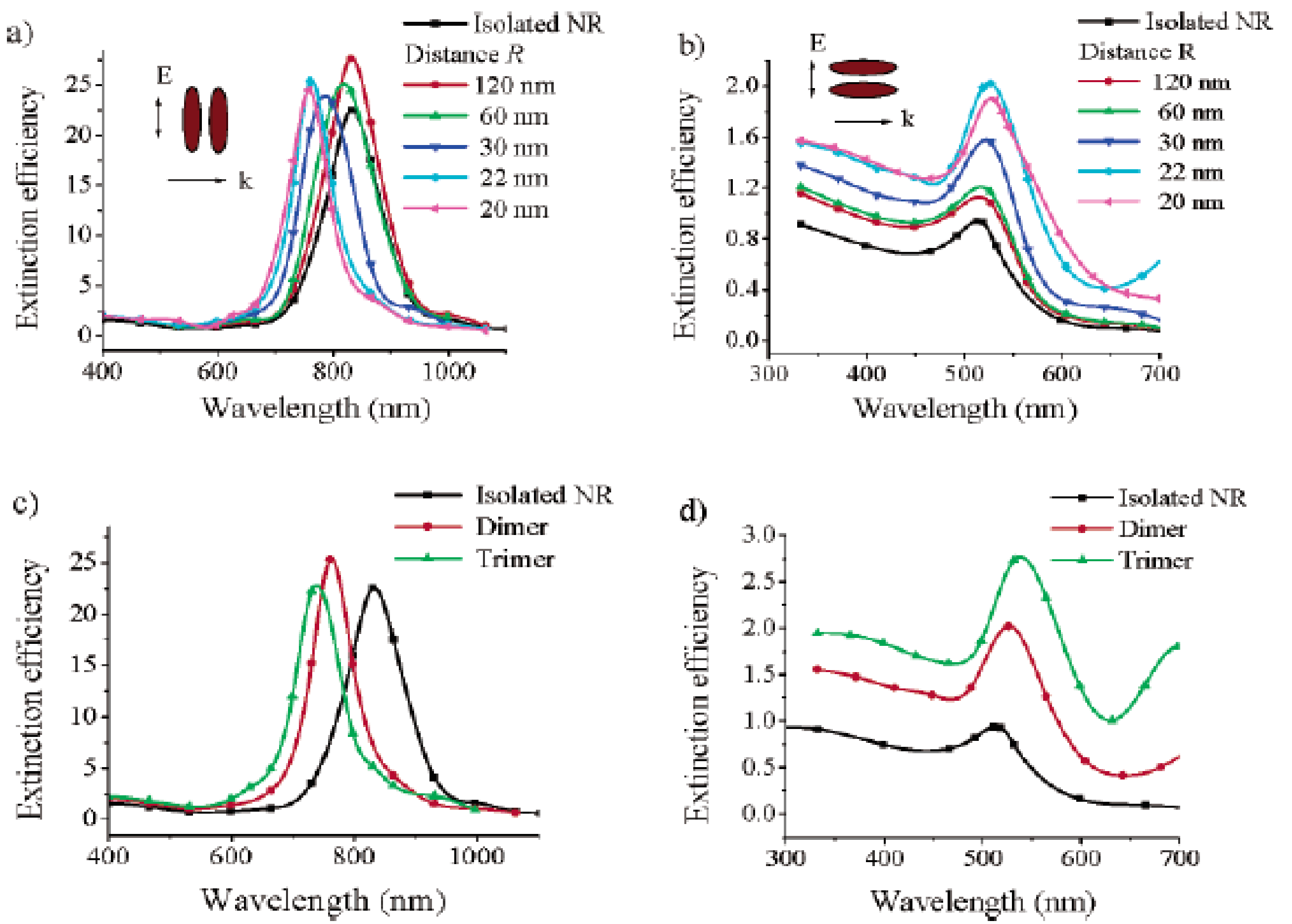

结果：在光场偏振垂直于纳米棒间的中心连线时，当棒间距离越近，蓝移得越远；当增加棒的个数时，蓝移得越远。

Plasmon Coupling in Nanorod Assemblies: Optical Absorption, Discrete Dipole Approximation Simulation, and Exciton-Coupling Model，Prashant K. Jain et al, J. Phys. Chem. B (2006) 110, 18243-18253

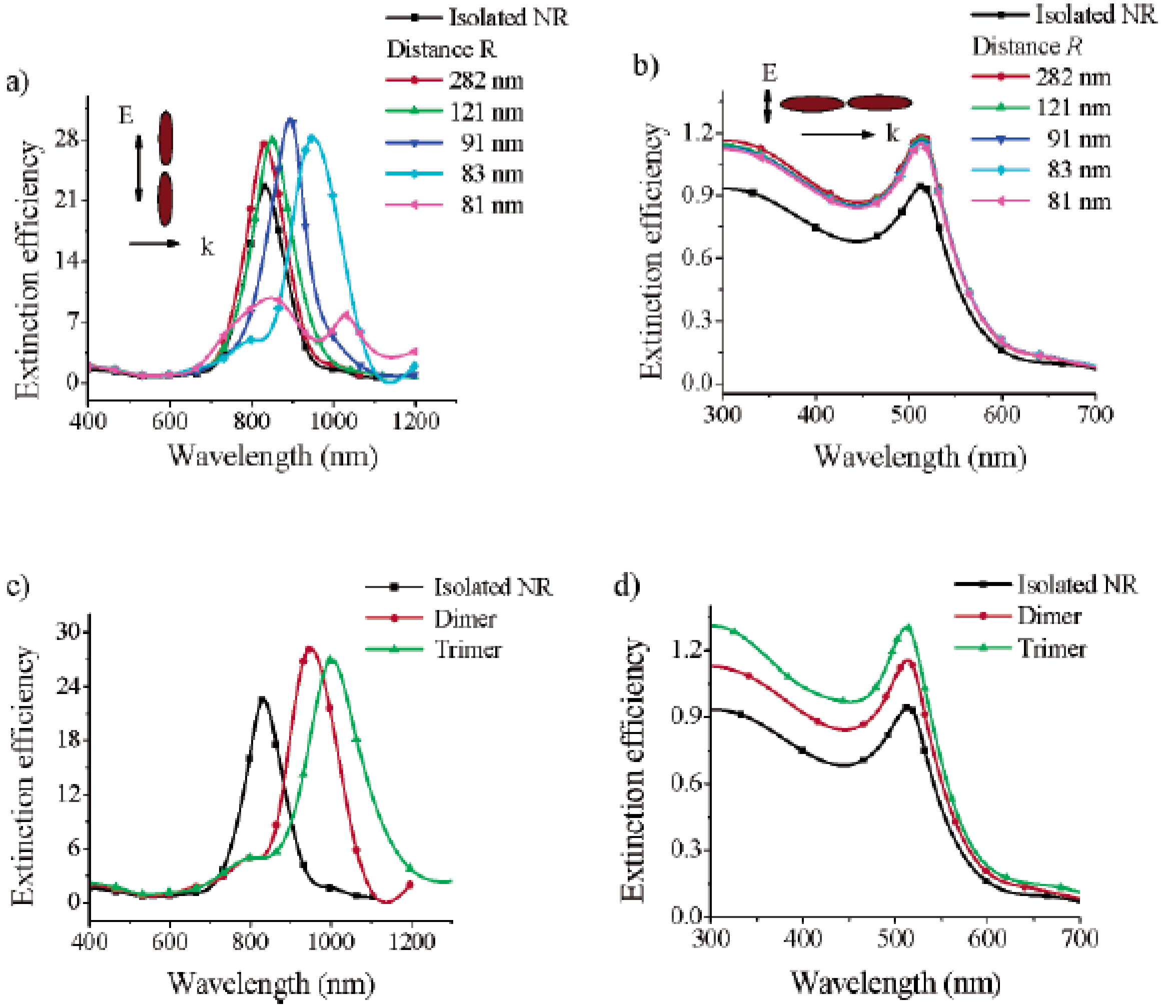

结果：在光场偏振平行于纳米棒间的中心连线时，当棒间距离越近，红移得越远；当增加棒的个数时，红移得越远。

[Plasmon Coupling in Nanorod Assemblies: Optical Absorption, Discrete Dipole Approximation Simulation, and Exciton-Coupling Model]

Prashant K. Jain et al, J. Phys. Chem. B (2006) 110, 18243-18253

纳米金属颗粒间SPR耦合的标度律

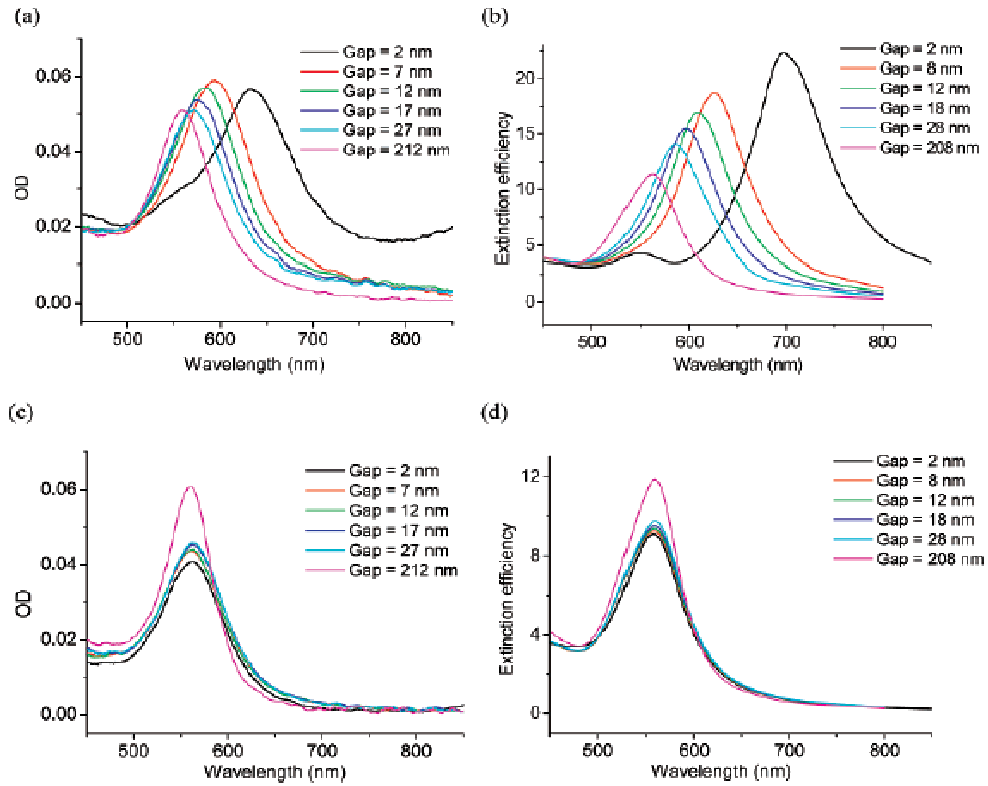

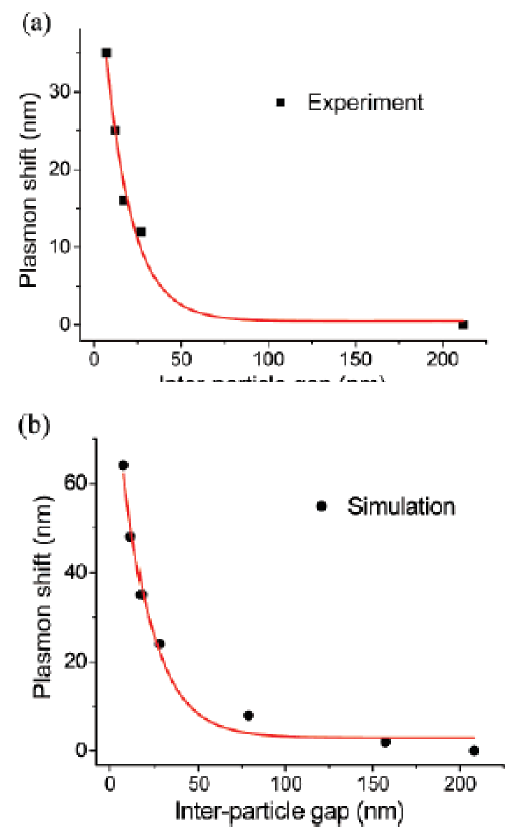

结果：从两个样品的吸收和消光峰以及理论和实验上共振峰移动规律，可以得到标度律 $\frac{\Delta\lambda}{\lambda_0} \approx 0.18 \exp\left(\frac{-(s/D)}{0.23}\right)$

On the Universal Scaling Behavior of the Distance Decay of Plasmon Coupling in Metal nanoparticle Pairs: A Plasmon Ruler Equation

Prashant K. Jain et al, NANO LETTERS (2007) Vol. 7, No. 7,2080-2088

用纳米金球壳结构的SPR收集太阳能

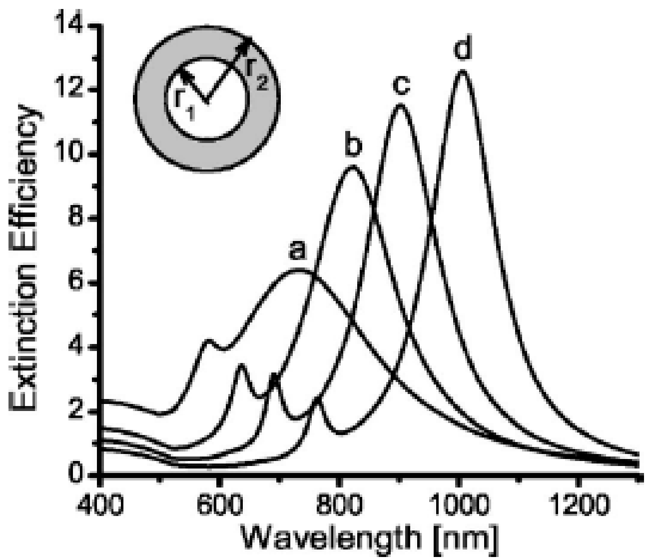

FIG. 1. Plasmon resonances of silica/Au nanoshell structures in water with r_1=60 nm and r_2= (a) 80 nm, (b) 70 nm, (c) 67 nm, and (d) 65 nm, respectively.

结果：通过调节纳米金球壳的核壳比例，其SPR的吸收谱可以覆盖太阳光的区域，用于solar cell。

Optimized plasmonic nanoparticle distributions for solar spectrum harvesting
Joseph R. Cole et al, APPLIED PHYSICS LETTERS 89, 153120 (2006).

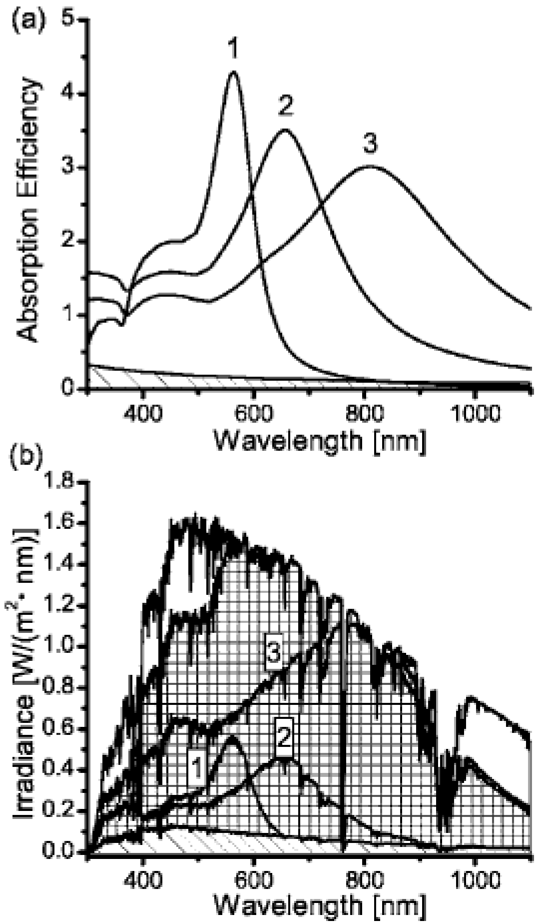

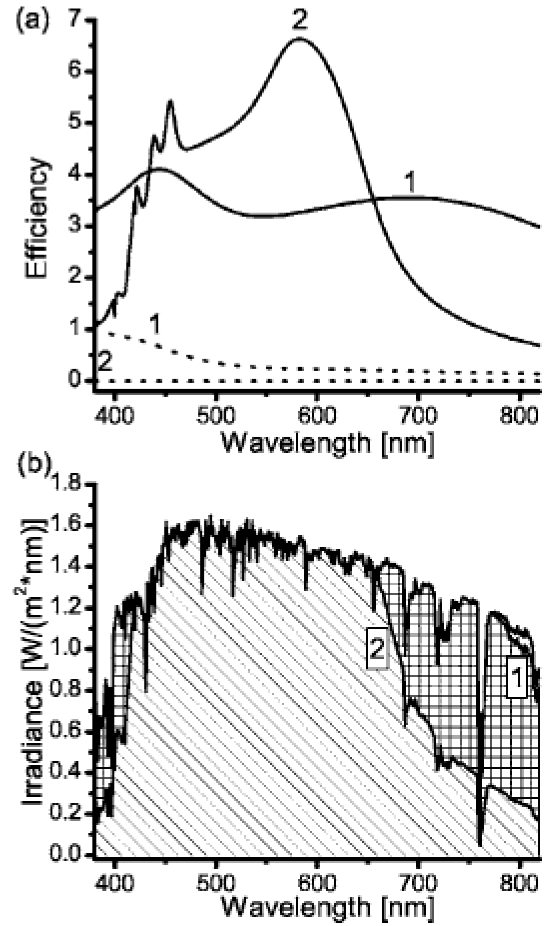

结果：将不同尺度的金或银球壳混合在一起，使其共振谱覆盖太阳光区域（**200nm～1500nm**），用于**solar cell** 能量收集。

Optimized plasmonic nanoparticle distributions for solar spectrum harvesting
Joseph R. Cole et al, APPLIED PHYSICS LETTERS 89, 153120 (2006).

纳米银膜上岛状结构的SPR实现二次谐波

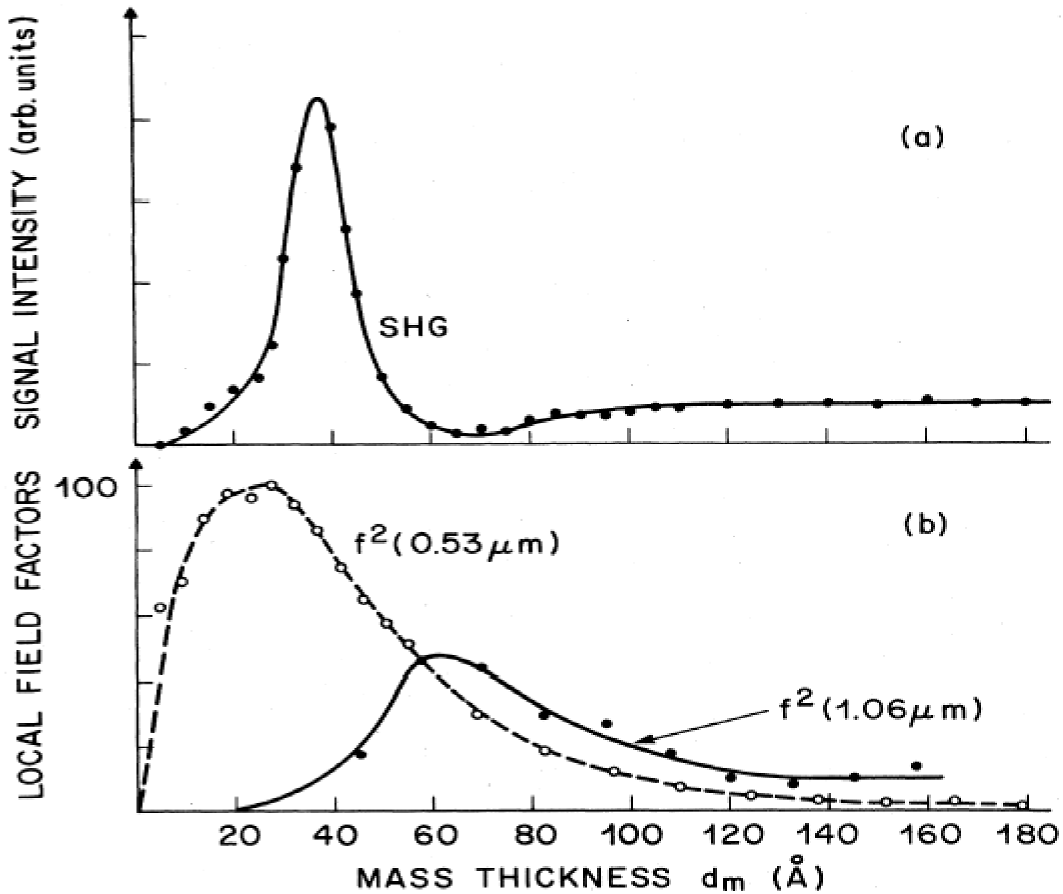

结果：SPR用于非线性光学的典型例子。可以看到，1060nm处激发，在530nm处产生了二次谐波。

Surface second-harmonic generation from metal island films and microlithographic strucures

A. Wokaun et al, PRB 24, 849 (1981)

纳米银岛上利用SPR实现三次谐波

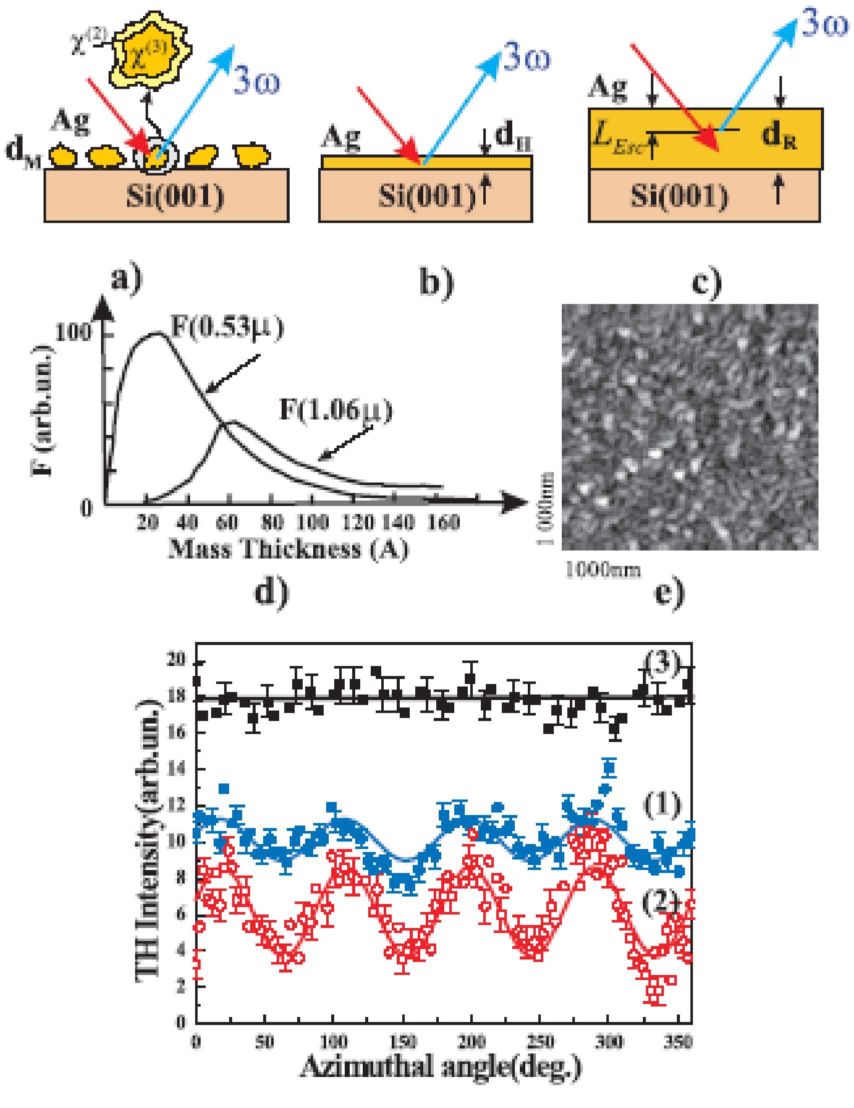

结果：SPR用于非线性光学的又一例子。入射波长1060nm，可以看到，（d）中产生的530nm二次谐波，(f) 中产生了355nm的三次谐波，厚度40nm时增益最强。

Surface-Enhanced Optical Third-Harmonic Generation in Ag Island Films

E. M. Kim et al, PRL 95, 227402 (2005)

利用纳米金球的SPR耦合实现多波混频

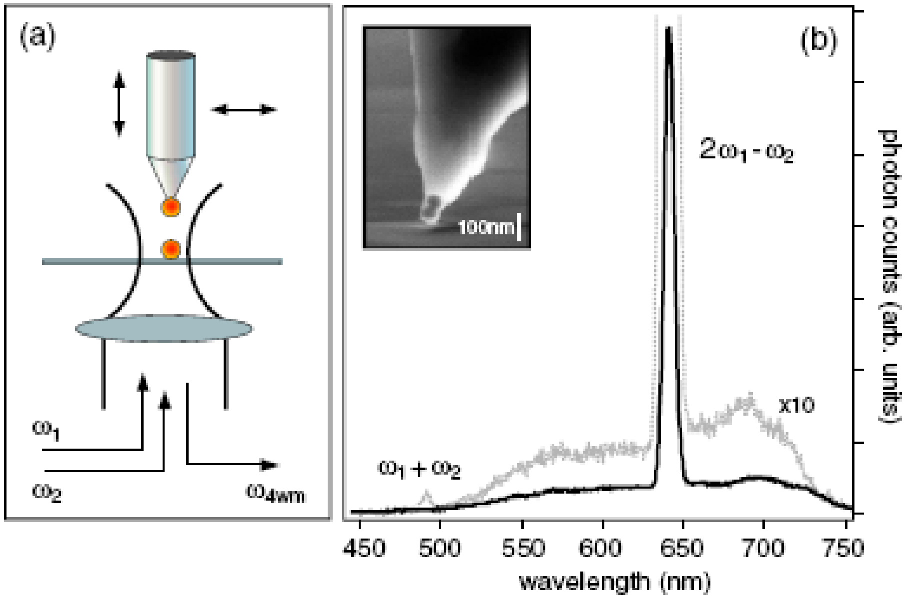

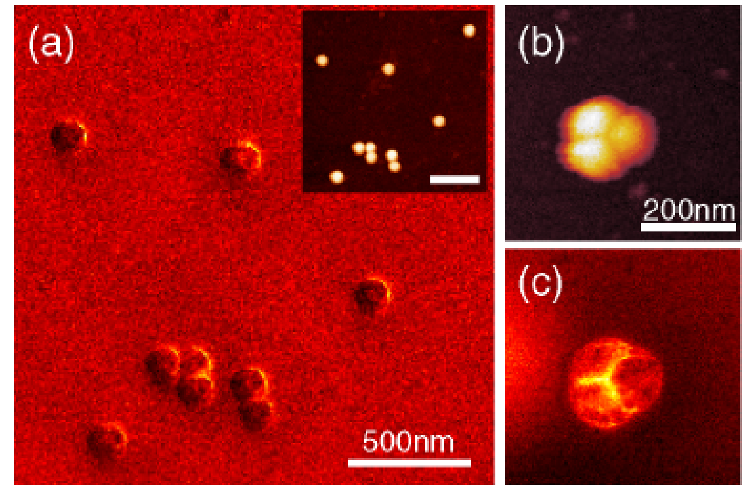

FIG. 1 (color online). (a) Sketch of the experiment. The nonlinear signal at frequency $2\omega_1 - \omega_2$ is measured as a function of the relative position between individual gold nanoparticles. (b) Emission spectrum from a dimer of two identical particles (60 nm diameter), excited with pulsed lasers of wavelength $\lambda_1 =$ 830 nm and $\lambda_2 =$ 1185 nm. The superimposed dotted curve shows the spectrum for two particles of unequal size (60 nm and 100 nm diameter). The inset shows an SEM image of two gold particles attached to a pointed optical fiber.

结果：SPR用于非线性光学的例子。实现多波混频。

[Optical Frequency Mixing at Coupled Gold Nanoparticles]

Matthias Danckwerts and Lukas Novotny, PRL 98, 026104 (2007)

利用纳米金属颗粒SPR实现生物传感

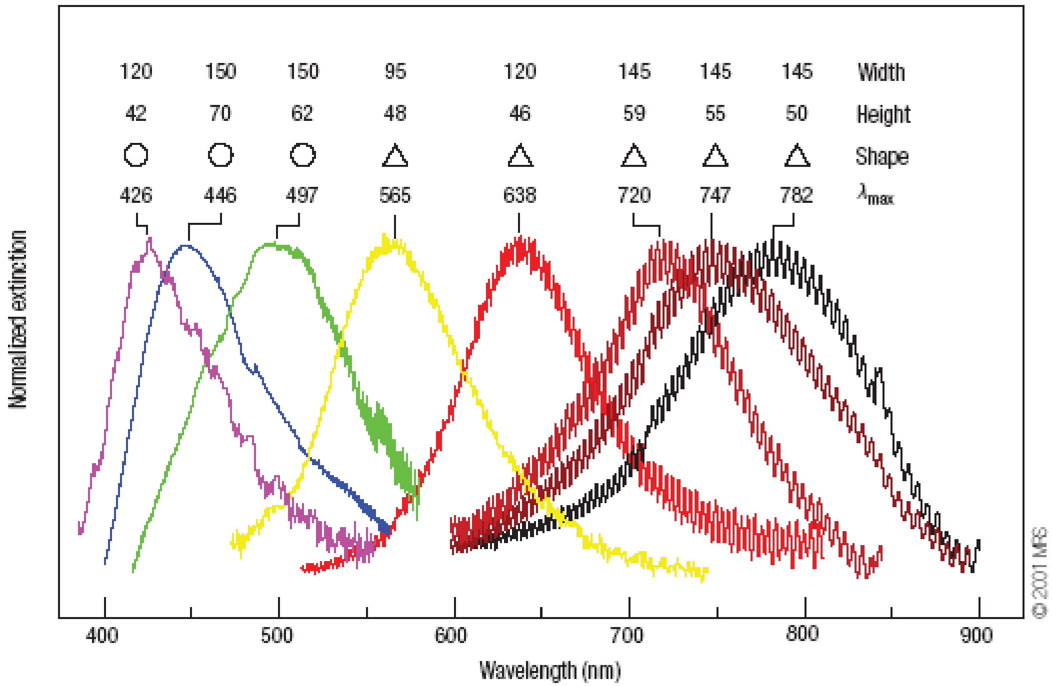

[Biosensing with plasmonic nanosensors]()

Jeffrey N. ANker et al，nature materials | VOL 7 | JUNE 2008|442

用纳米近颗粒的SPR实现数据存储

Aim to: **minimize the recording storage by multiplexing: wavelength, polarization, and spatial dimensions**

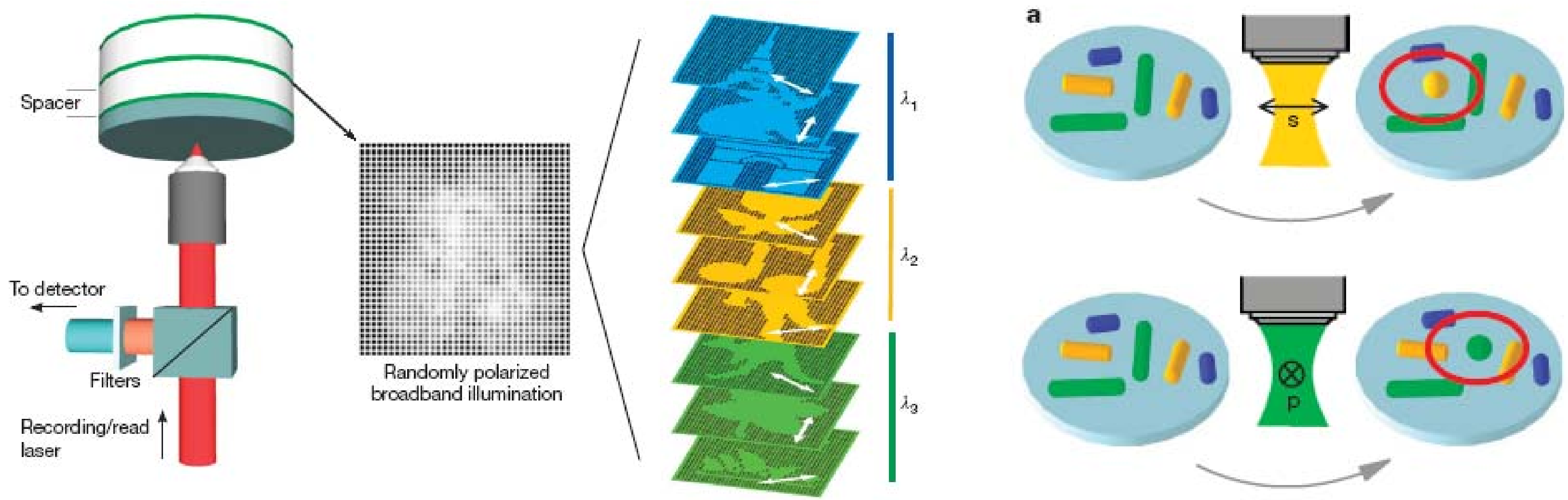

Results:

realizing five-dimensional data recording by SPR

[Five-dimensional optical recording mediated by surface plasmons in gold nanorods]
M. Gu et al, NATURE|Vol 459|410| 2009

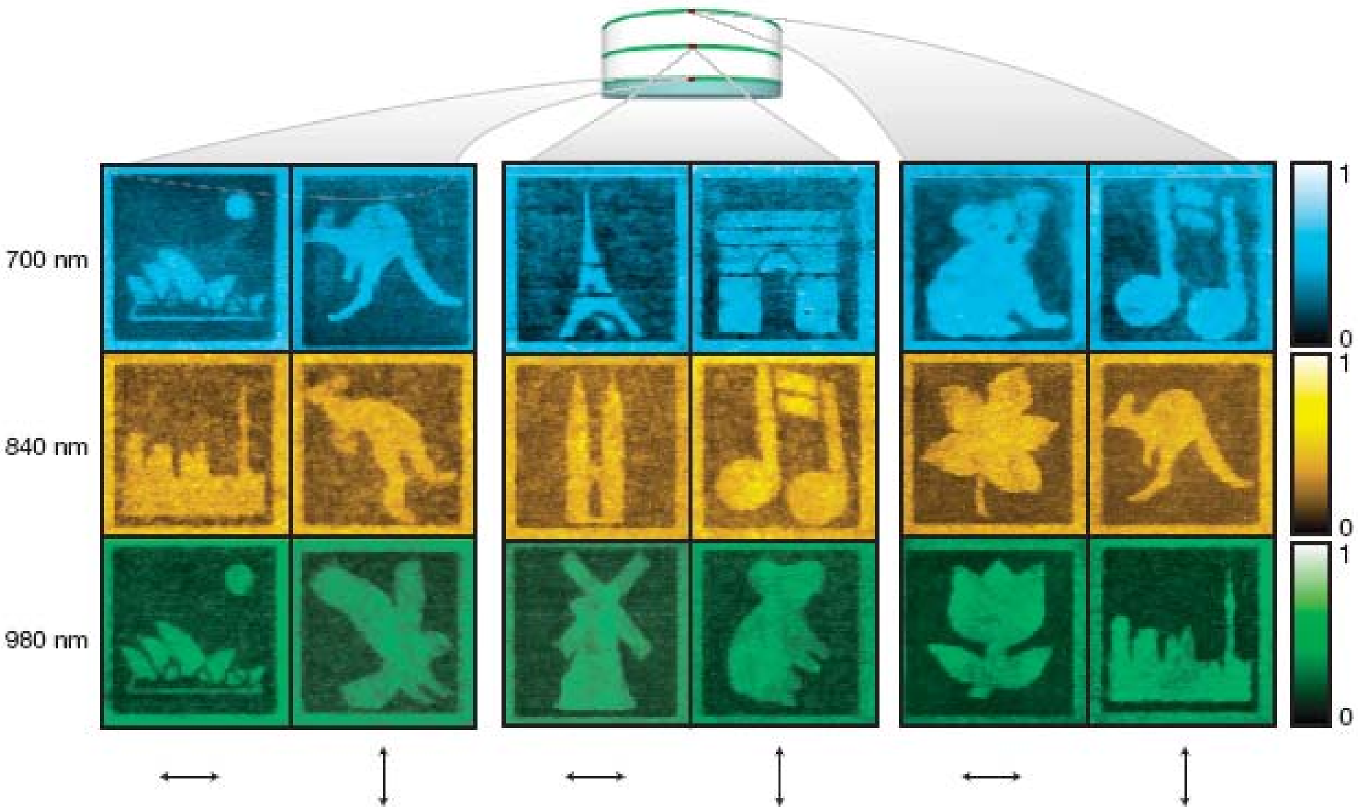

Results:

realizing five-dimensional data recording by SPR

Five-dimensional optical recording mediated by surface plasmons in gold nanorods

M. Gu et al, NATURE|Vol 459|410| 2009

4.2 表面等离激元（SPP）波导

类型：平面波导、槽形波导、柱形波导、球链波导、弯形波导、金属介质混合型波导 (杂化波导)

特点：结构的尺度在亚波长范围内、电场束缚在金属表面、传播长度有限

用途：分束器、干涉仪等纳米的光子器件

意义：实现器件的小型化、信息传输速度快、各种光子器件的基础

纳米金属条形SPP波导

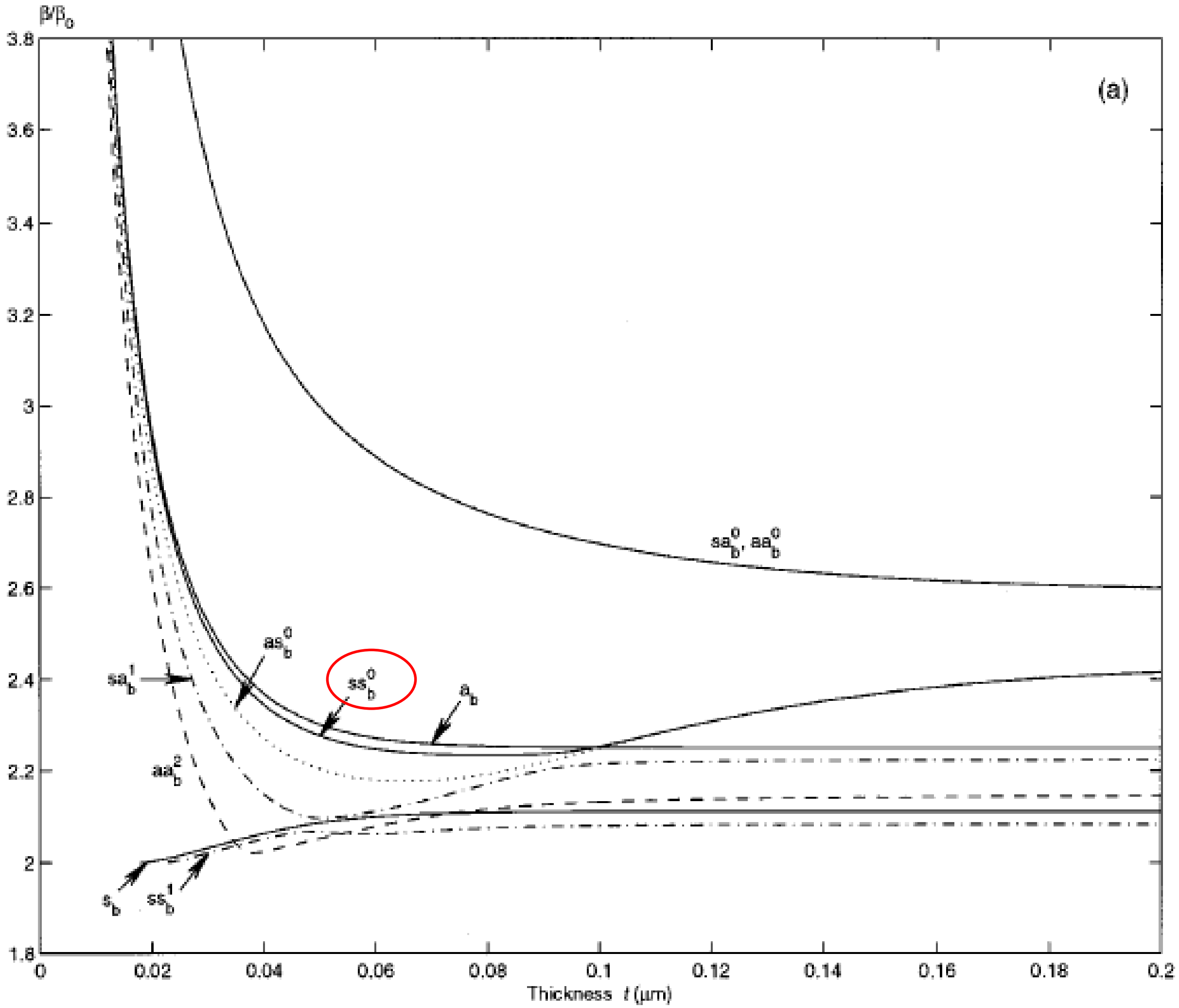

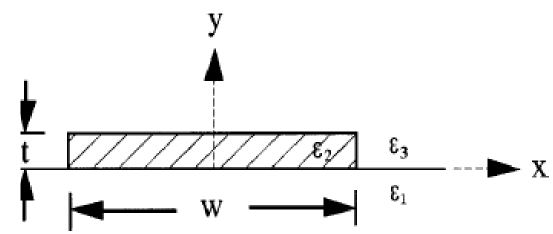

传播常数的实部

关于**x**和**y**对称和反对称共有**4**支**SP**模式。

Plasmon-polariton waves guided by thin lossy metal films of finite width: Bound modes of asymmetric structures, **Pierre Berini, PHYSICAL REVIEW B, VOLUME 63, 125417 (2001).**

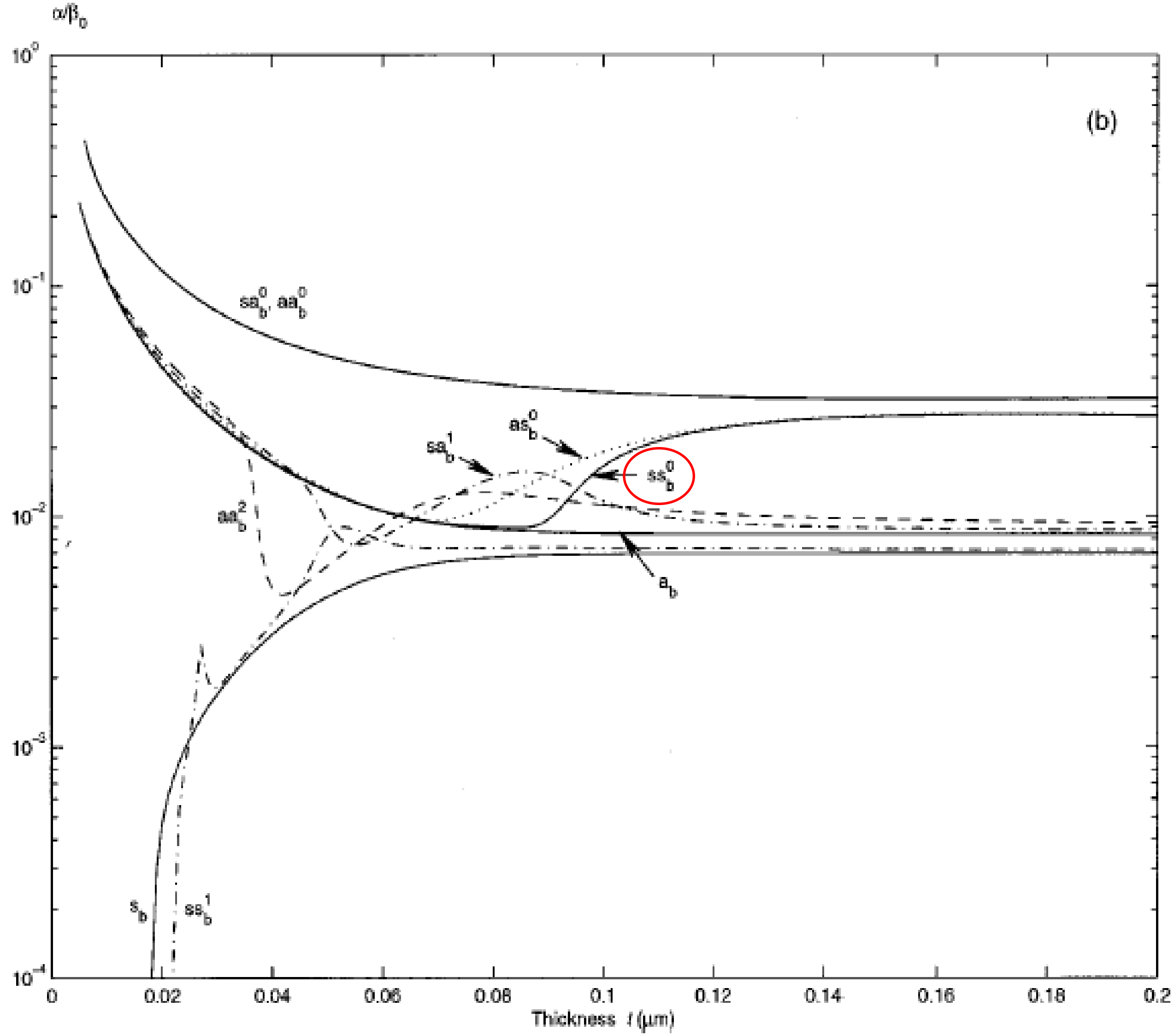

传播常数的虚部

[Plasmon-polariton waves guided by thin lossy metal films of finite width: Bound modes of asymmetric structures,]() **Pierre Berini, PHYSICAL REVIEW B, VOLUME 63, 125417 (2001).**

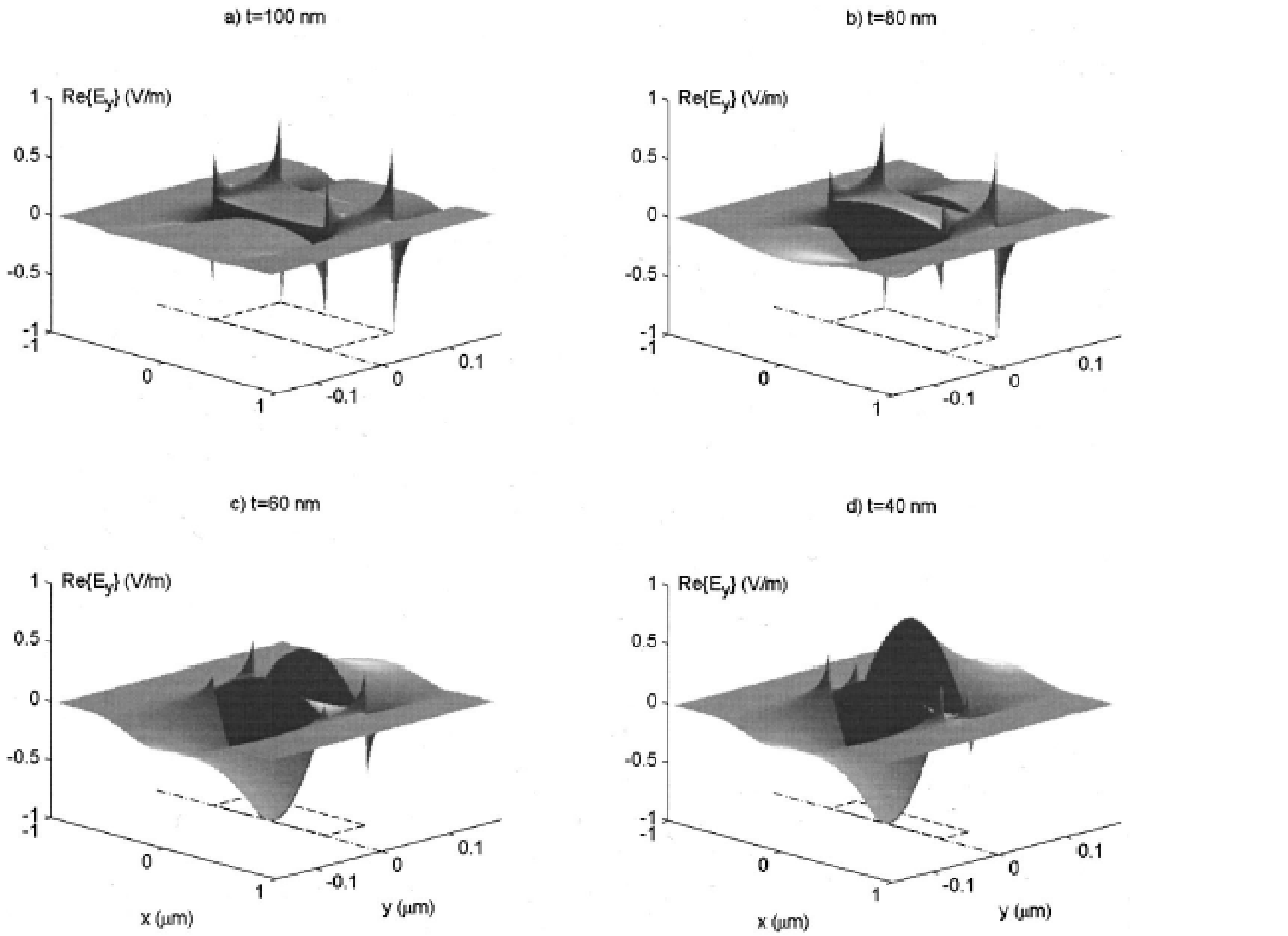

SS_b^0在宽度是1um厚度变化时的Ey电磁场分布

厚度薄的时候倏逝波特征明显

Plasmon-polariton waves guided by thin lossy metal films of finite width: Bound modes of asymmetric structures, **Pierre Berini, PHYSICAL REVIEW B, VOLUME 63, 125417 (2001).**

槽形SPP波导

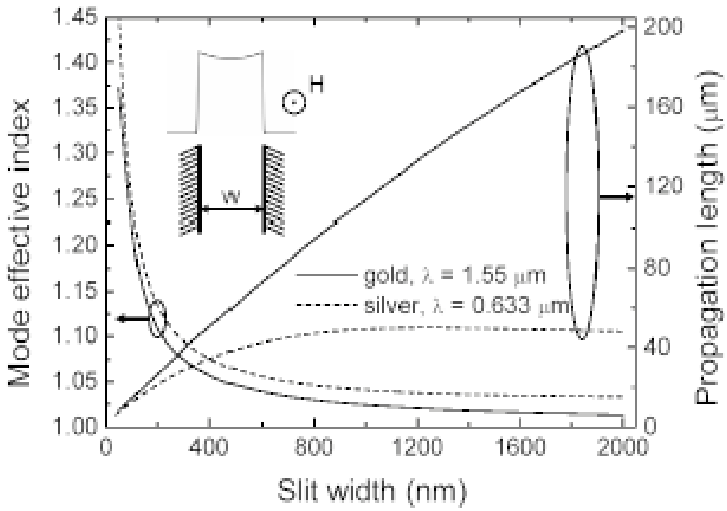

FIG. 1. The S-SPP (symmetric) mode effective index and i...

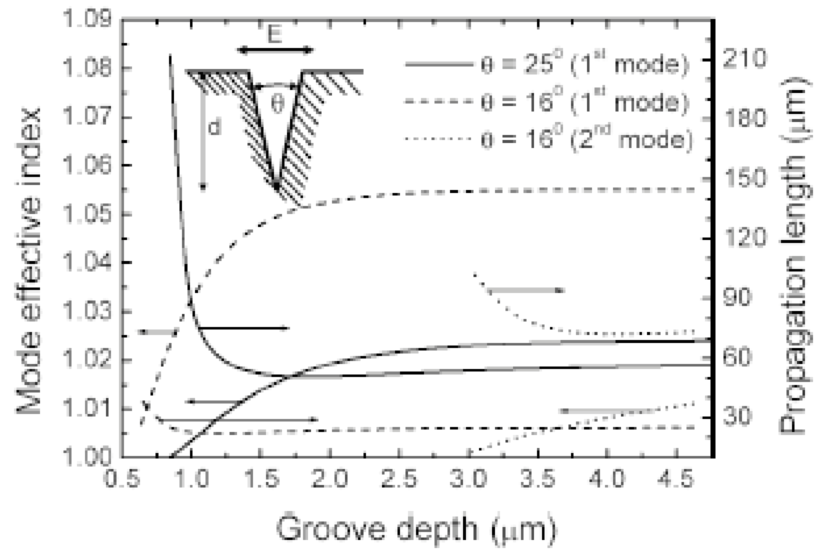

想法：与MIM型波导的比较的角度去理解，以期找到局域性好传播又长的模式。

Channel Plasmon-Polariton Guiding by Subwavelength Metal Grooves,
Sergey I. Bozhevolnyi et al, PRL 95, 046802 (2005)

槽形SPP波导中电场

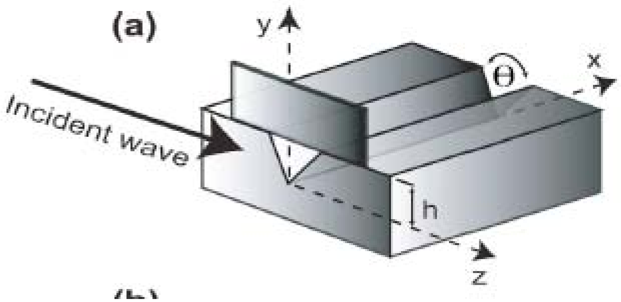

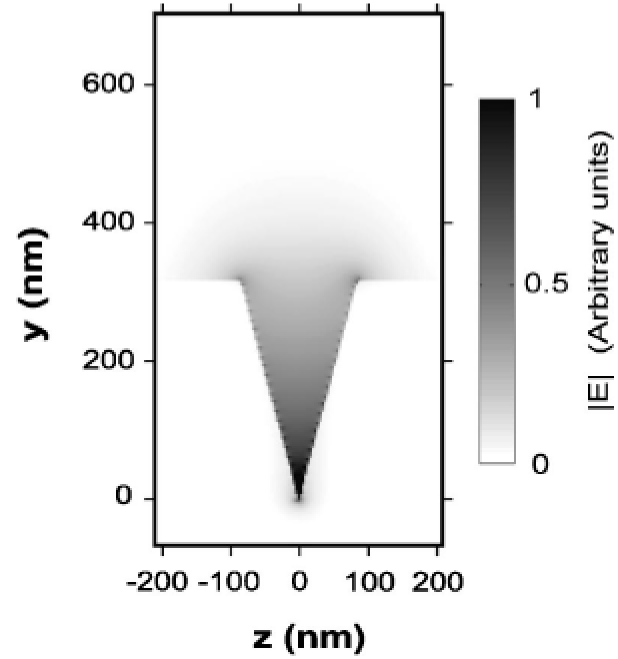

可以看到：在以金属为基底的槽形波导中，模式的能量集中在槽中，利于导波。

Single-mode subwavelength waveguide with channel plasmon-polaritons in triangular grooves on a metal surface，D. K. Gramotnev and D. F. P. Pilea, Appl. Phys. Lett., Vol. 85, 6323 (2004).

Channel SPP waveguide components including interferometers and ring resonators
T. W. Ebbesen et al, 2006 （第一章中提过）

challenge to: the miniaturization and high-density integration of optical circuits at telecom. Wavelength

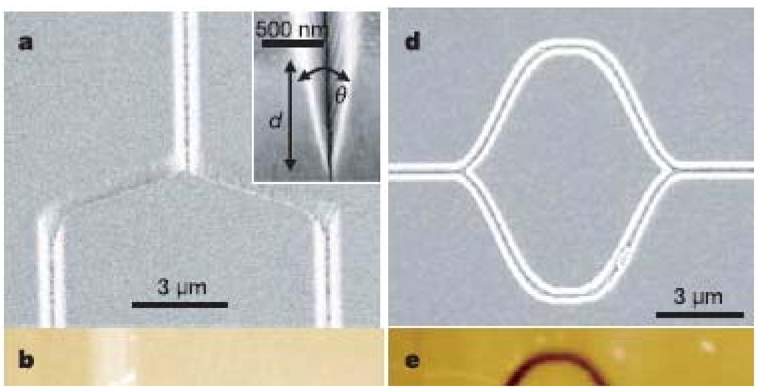

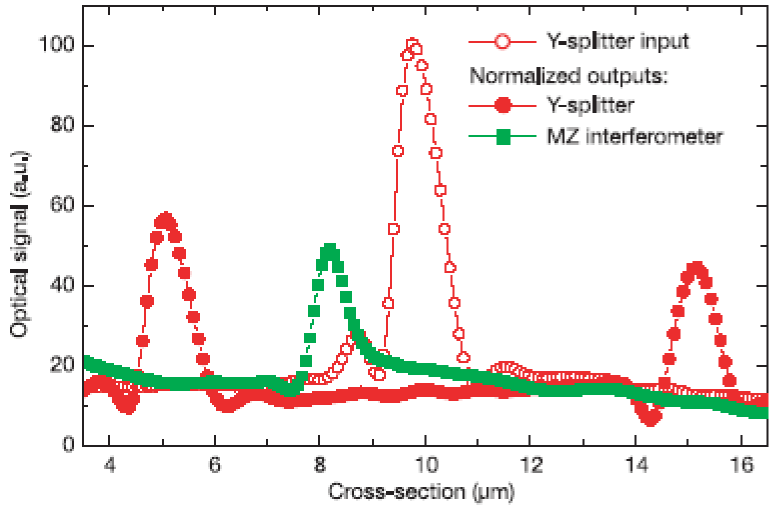

Results:
Grooves in silver, strong light confinement, low propagation loss

Significance:
nano devices based Channel SPP

Channel plasmon subwavelength waveguide components including interferometers and ring resonators, T.W. Ebbesen et al, NATURE|Vol 440|508| 2006

柱形SPP波导（一维）

金属纳米线

- 对每个n，存在表面模式TM_0，HE_n。

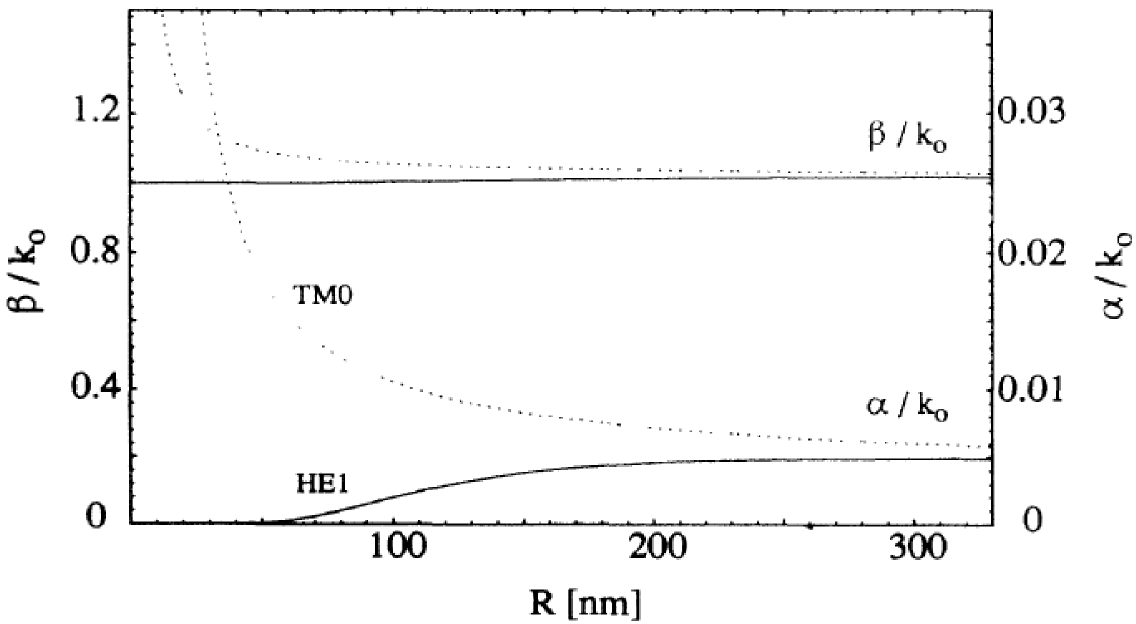

铝纳米线，波长488nm

L. Novotny et al, Phys. Rev. E 50, 4094 (1994).

金属纳米管

- HE_1表面模式
- 众多波导模式HE_{1n}，在管内径减小截止。
- 表面模式和波导模式之间存在模式转换现象。

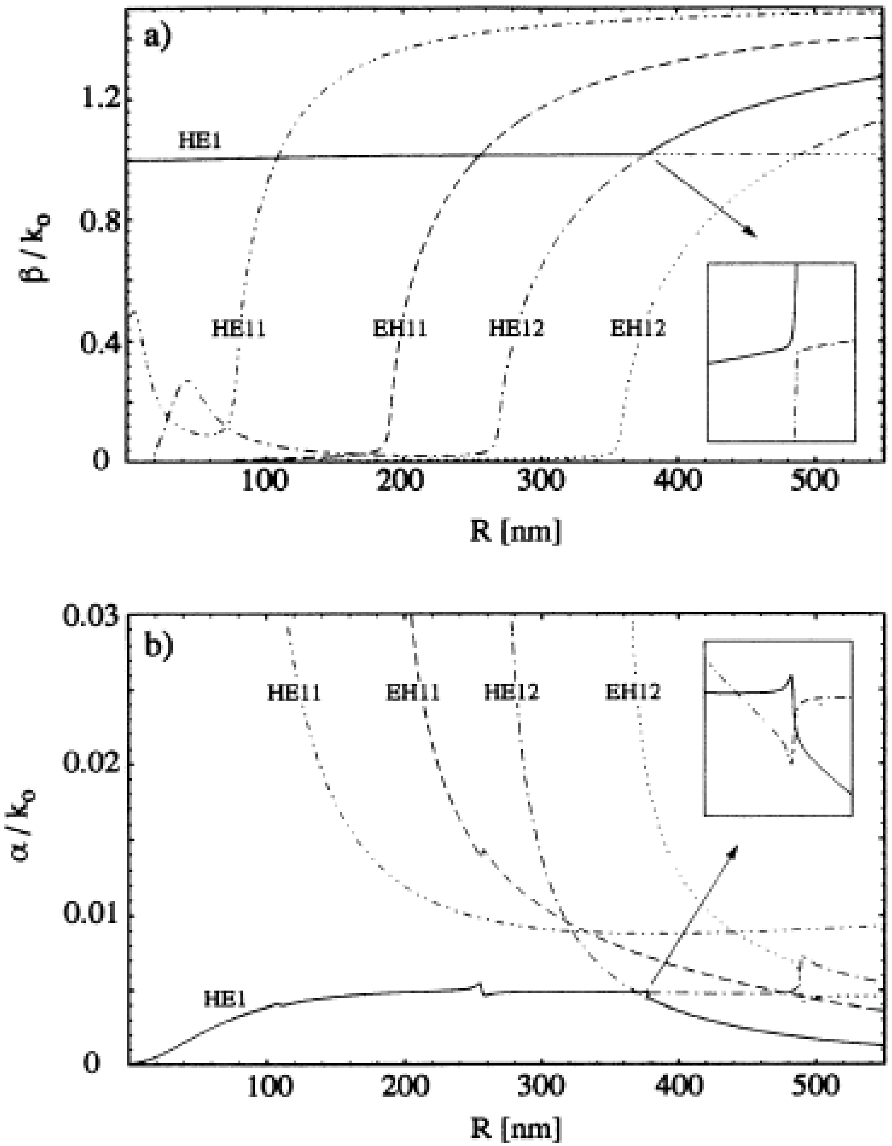

L. Novotny et al, Phys. Rev. E 50, 4094 (1994).

球链SPP波导

原理：通过纳米金属颗粒间的近场耦合实现光的传递

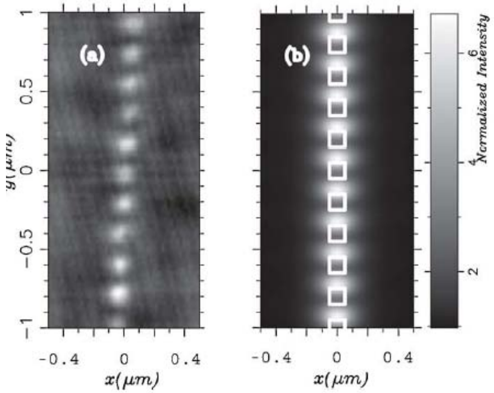

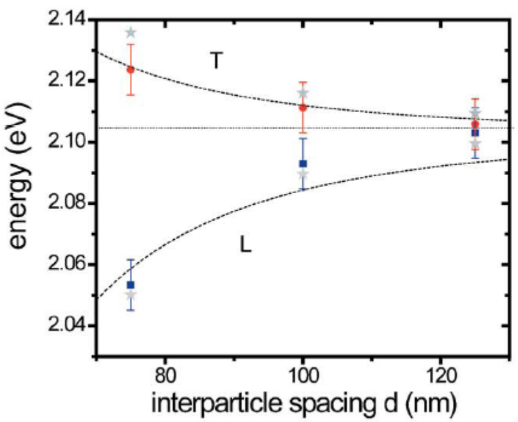

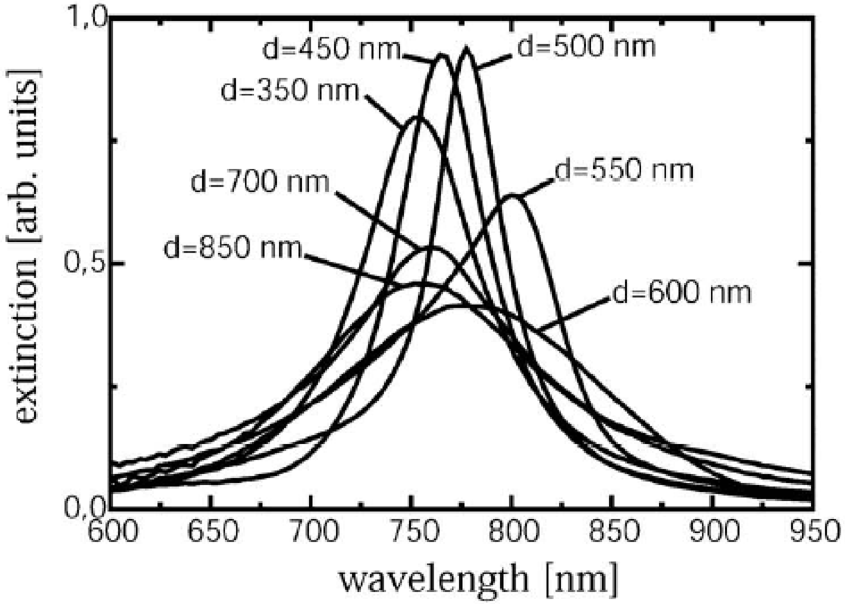

可以看到：由于小球上电场偏振的不同而出现**T**模式和**L**模式；
小球间距离的不同导致消光峰的位置不同。

Plasmonics: Localization and guiding of electromagnetic energy in metal/dielectric
Stefan A. Maier and Harry A. Atwater, JOURNAL OF APPLIED PHYSICS 98, 011101 2005

聚焦后用SPP波导传输

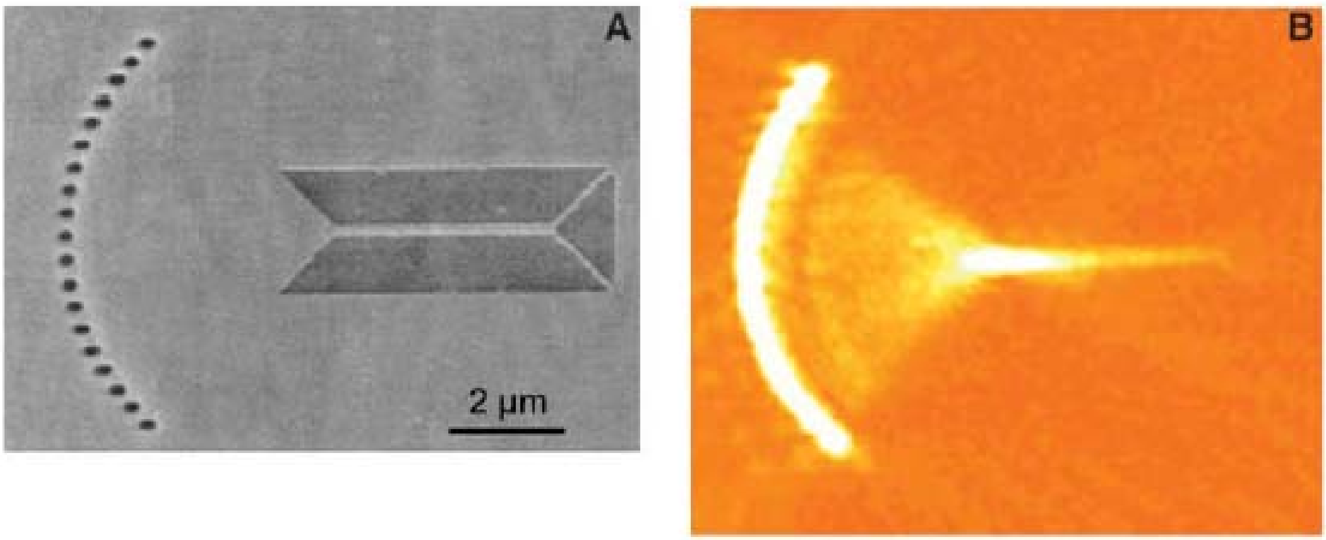

Fig. 2. (**A**) SEM image of a nanodot focusing array coupled to a 250-nm-wide Ag strip guide. (**B**) NSOM image of the SP intensity showing subwavelength focusing. [Adapted from (*15*)]

原理：如上图所示，光场通过半圆排列的纳米小洞后聚焦，聚焦后的能量通过SPP波导传递。

Plasmonics: Merging Photonics and Electronics at Nanoscale Dimensions

Ekmel Ozbay,SCIENCE VOL 311,189, 2006

弯形SPP波导

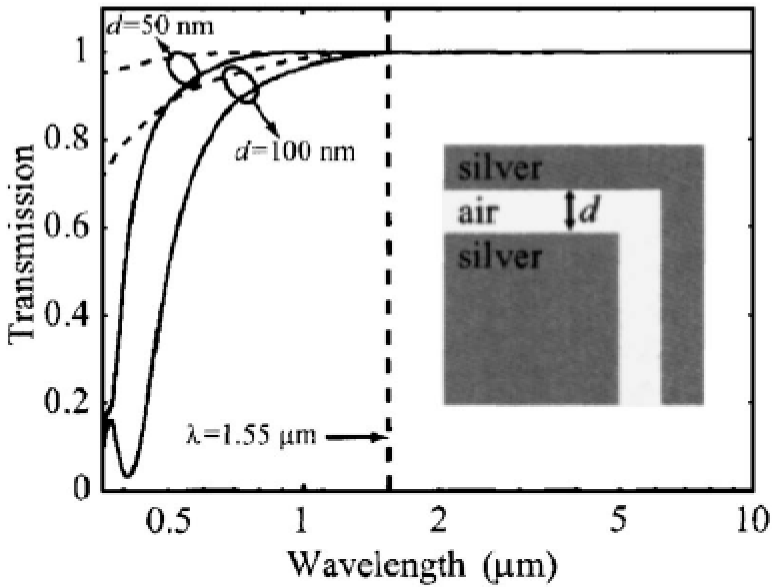

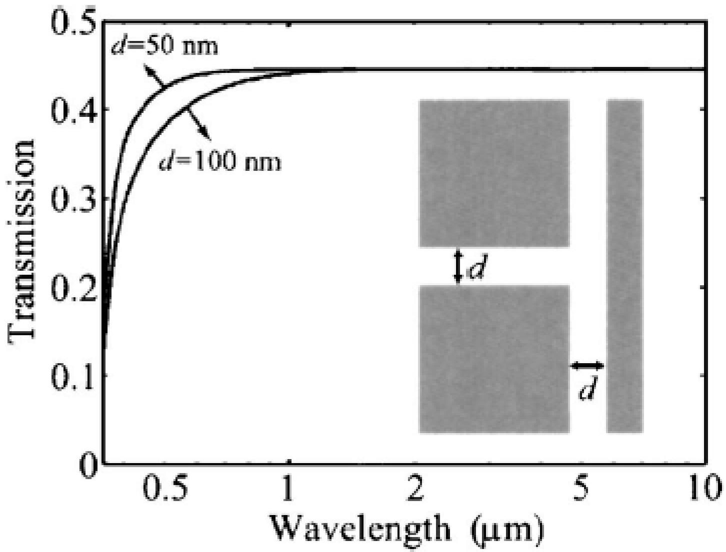

结果：如上图所示，SPP通过弯形波导和T型分束器后，透射率很高。

Bends and splitters in metal-dielectric-metal subwavelength plasmonic waveguides
Georgios Veronis and Shanhui Fan， APPLIED PHYSICS LETTERS 87, 131102 (2005).

金属介质混合型波导

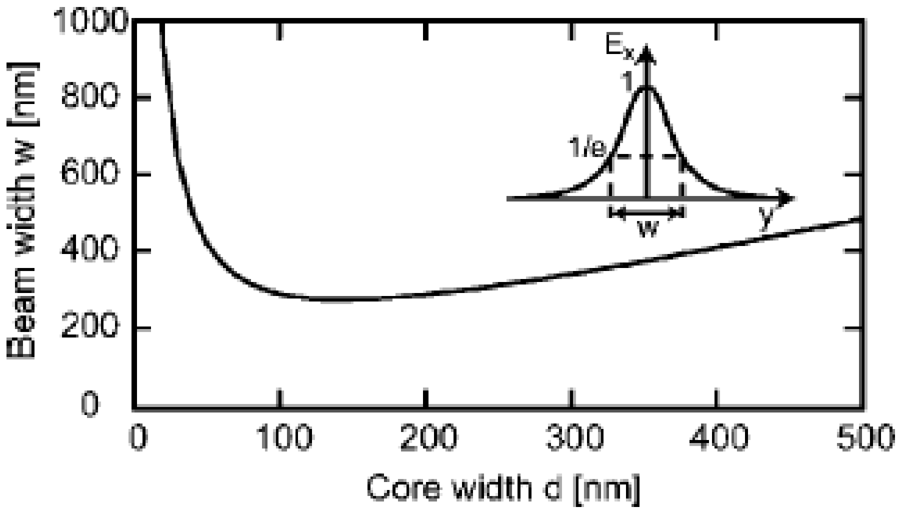

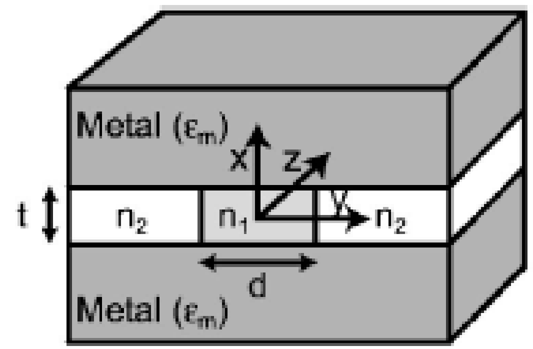

632nm, Au

n_1=1.45,n_2=1.0

t=100nm

结果:

将传播的**SP**进一步局域在宽度为**d**的介质条中。

Propagation properties of guided waves in index-guided two-dimensional optical waveguides

Fuminori Kusunokia et al, APPLIED PHYSICS LETTERS 86, 211101 (2005)

金属介质混合型波导

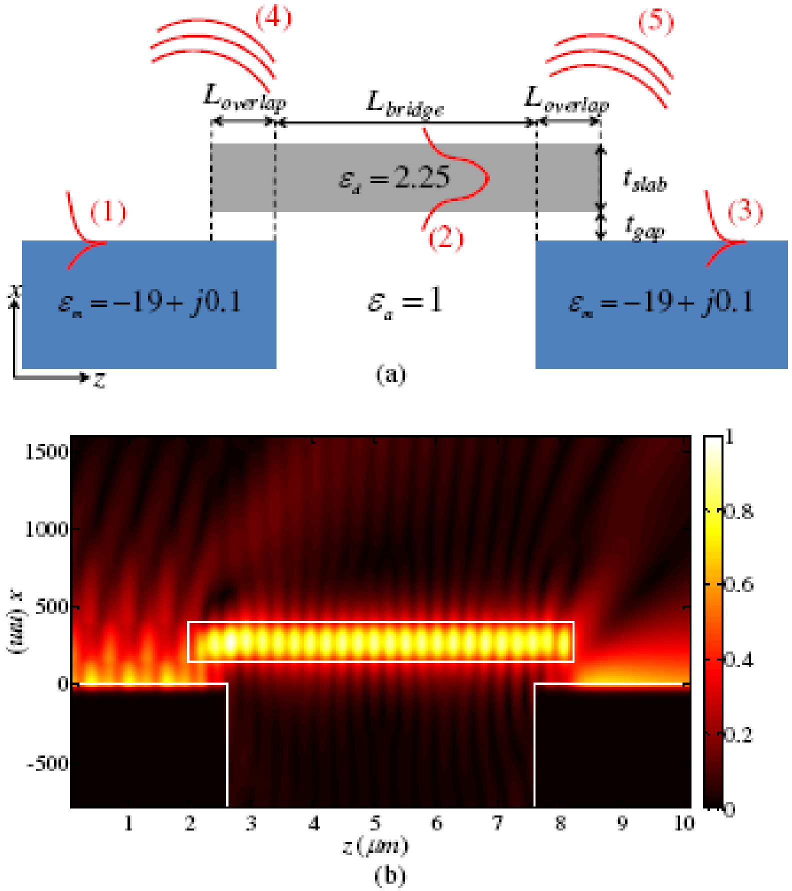

Fig. 1. (a) Schematic diagram of a floating dielectric slab interconnection between two air-based single metal-dielectric interface SPP waveguides. Each red drawing with number indicates corresponding eigenmode or scattered wave in given geometry. (b) (Media 1) The amplitude distribution of the magnetic field (H_y) of the floating dielectric slab interconnection; with t_{gap}=150 *nm*, t_{slab}=250 *nm*, $L_{overlap}$=600 *nm*, and L_{bridge}=5 *μm*, respectively.

结果:

通过近场耦合，将传播的SP的能量局域在介质条上。

Floating dielectric slab optical interconnection between metal-dielectric interface surface plasmon polariton waveguides，**Minsu Kang et al, OPTICS EXPRESS, 17,676 (2009).**

杂化SPP波导

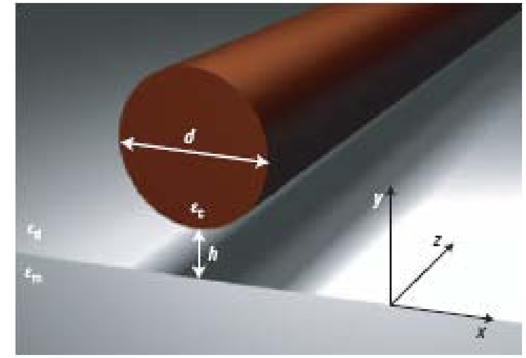

Sub-wavelength confinement and long-range propagation

Hybrid waveguide:
dielectric cylindrical nanowire
ε_C =12.25, d
dielectric gap n_c=2.25, h
metallic half-space Ag

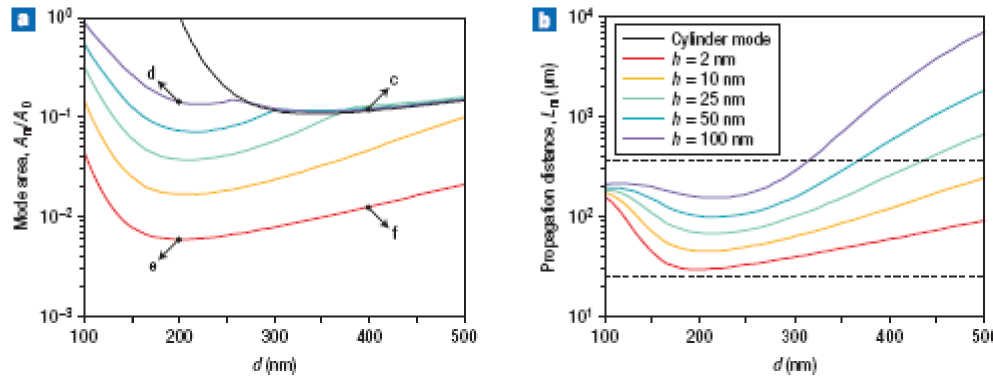

Results:
tightly confined field in the vicinity of the gap,low-loss light transport

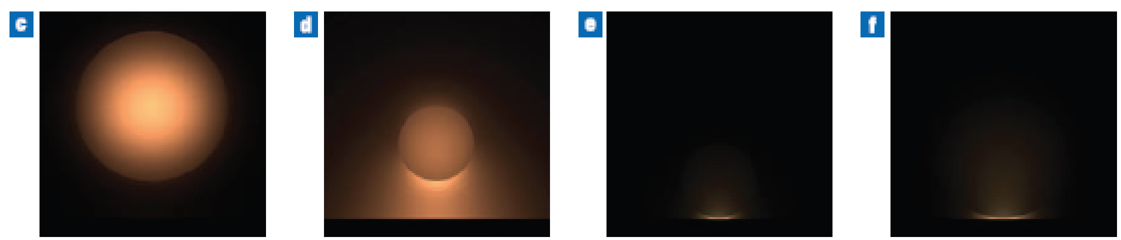

Explanation:
Hybridization of the fundamental mode of a dielectric cylinder with the SPP of a dielectric-metal interface.

A hybrid plasmonic waveguide for subwavelength confinement and long-range propagation, R. F. Oulton, et al, Nature Photon. 2 (2008) 496

杂化SPP波导

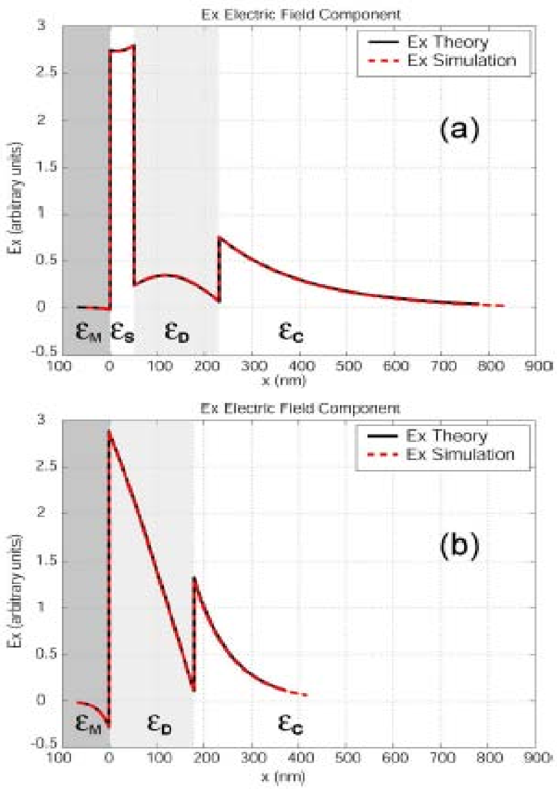

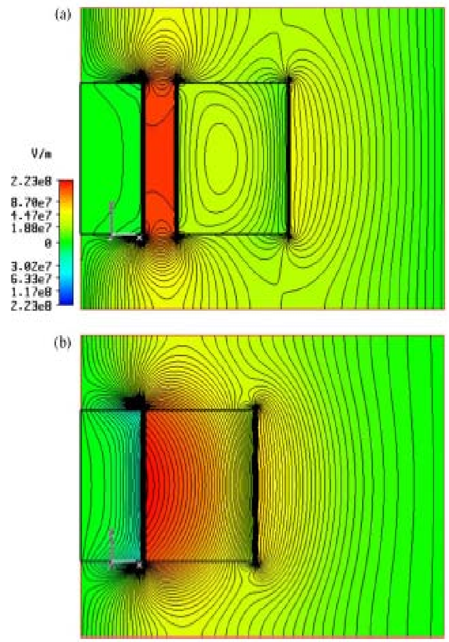

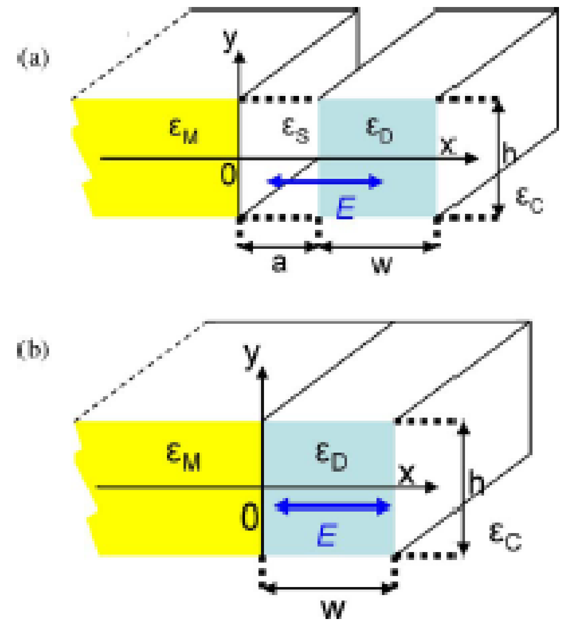

参数：

$\varepsilon_S = \varepsilon_C = 1, \varepsilon_D = 11.9, \varepsilon_M = -115.8 + j10.33.$

$h = 200$ nm, $a = 50$ nm, $w = 180$

1550 nm.

结论：

电磁场被局域在gap中或高介电常数材料中

Analysis of Hybrid Dielectric Plasmonic Waveguides，Rub´en Salvador et al, IEEE JOURNAL OF SELECTED TOPICS IN QUANTUM ELECTRONICS, VOL. 14, 1496 (2008)

其它类型SPP波导

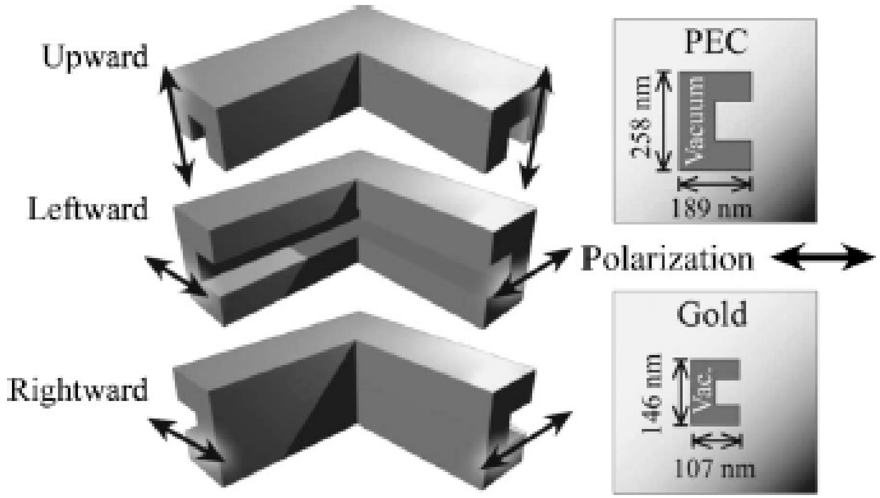

Fig. 1. Waveguide simulation schematic showing the possible orientations for a 90° bend in a C-aperture waveguide, as well as the cross-sectional dimensions of the simulated structures.

C型波导

Design of a subwavelength bent C-aperture waveguide,

Paul Hansen et al, OPTICS LETTERS,12,1737 (2007).

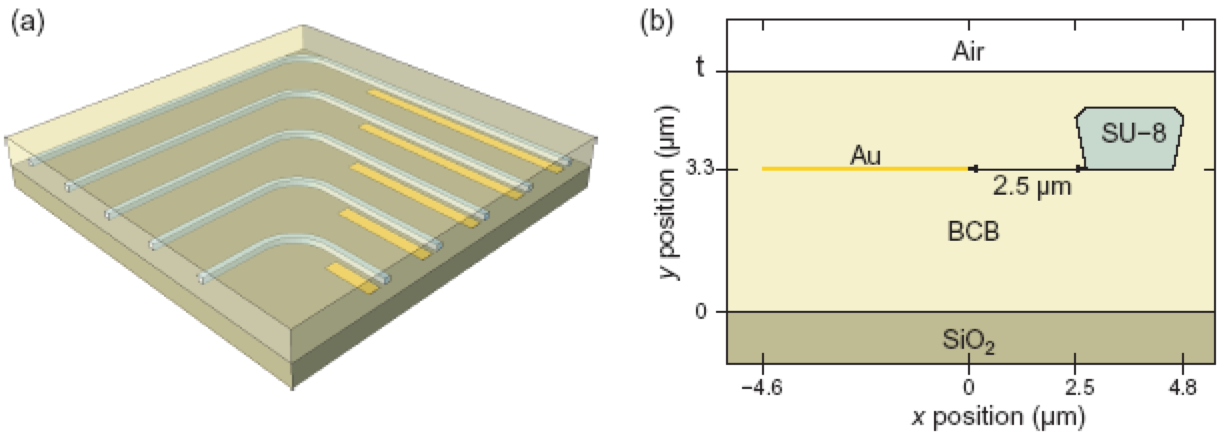

Figure 1. (a) Overview of the structures consisting of a series of SU-8 waveguides coupled to Au stripes. The radius of curvature of the SU-8 waveguides is 1 mm. (b) Cross-sectional view of a coupler. Except for the thickness *t* of the BCB layer, the coupler dimensions are kept constant throughout this study and the couplers are always positioned 3.3 μm above the SiO_2 substrate. The Au stripe has a width of 4.6 μm, a thickness of 36 nm, and is separated from the SU-8 waveguide by a gap of 2.5 μm. The average width and thickness of the SU-8 waveguide are 2 μm and 1.5 μm. At $\lambda = 1.55\ \mu$m, the permittivity of Au is $-132 + 12.65i$ [22] and the refractive indices of SiO_2, BCB and SU-8 are, respectively, 1.444 [20], 1.535 [21] and $1.57 + 8e - 5i$. Note that we have added an imaginary part to the refractive index of SU-8 so as to fit the losses of our real waveguides. These losses were determined with cut-back measurements.

弯型混合波导

Directional coupling between dielectric and long-range plasmon waveguides，
Aloyse Degiron et al, New Journal of Physics 11 (2009)

其它类型SPP波导（仅给出示意图）

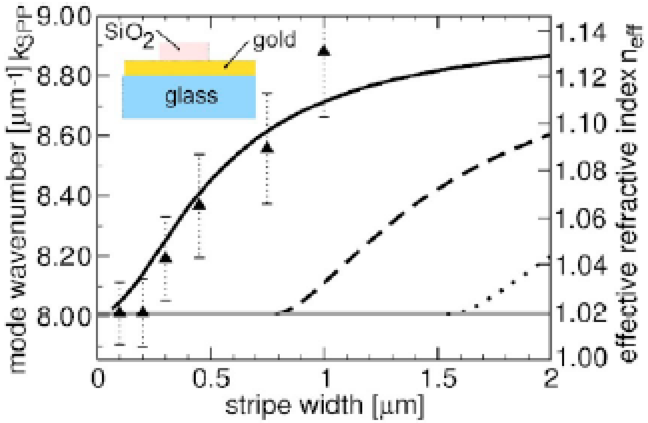

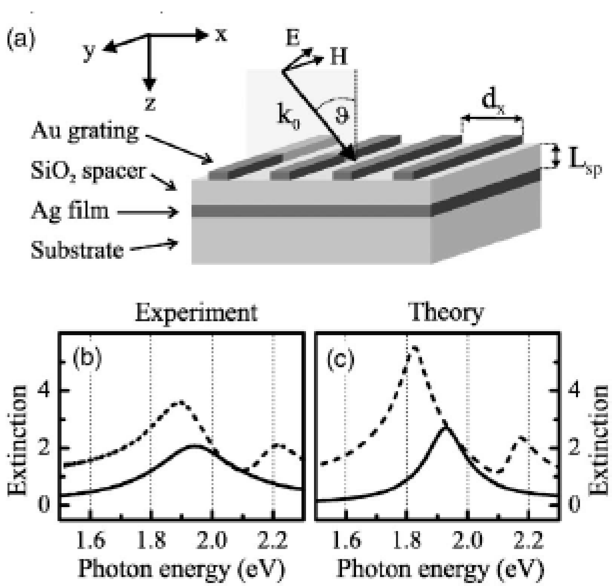

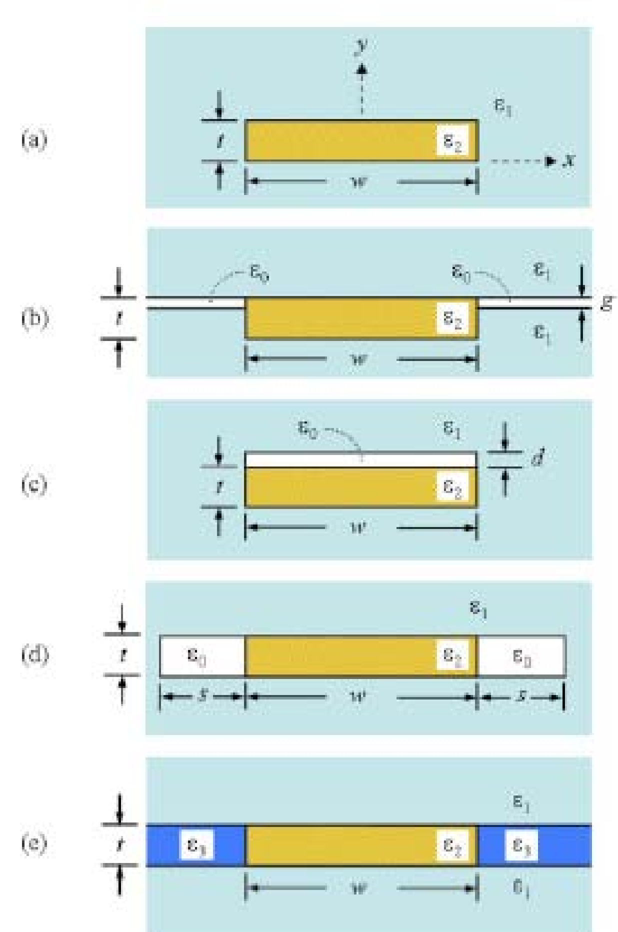

JOURNAL OF APPLIED PHYSICS 102, 033112 (2007); APPLIED PHYSICS LETTERS 88, 094104 (2006); PHYSICAL REVIEW B 74, 155435 (2006).

4.3 周期性结构中SPP性质

Comparisons

Photonic crystals:

spatially periodic dielectric structures

Photonic band gaps with a period ～ wavelength

To transmit and reflect light within specific frequencies

Properties tunable by the periodicity or refraction index

Polaritonic crystals: (periodical metallic nanostructure)

periodic arrangement of defects on a metal-dielectric interface

SPP band gaps with surface structure ～ wavelength of SPP

Scattering of SPP into SPP or SPP into light

(Extraordinary transmission from visible to microwave)

Properties tunable by the surface features

Dispersion relations

Photonic crystals:

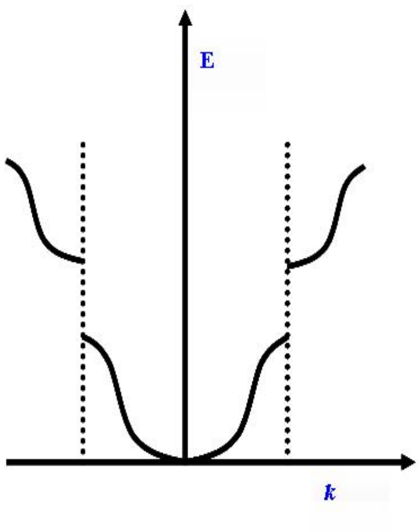

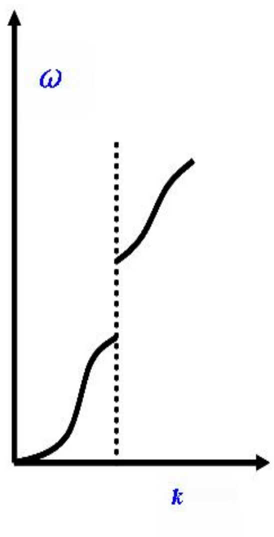

Polaritonic crystals:

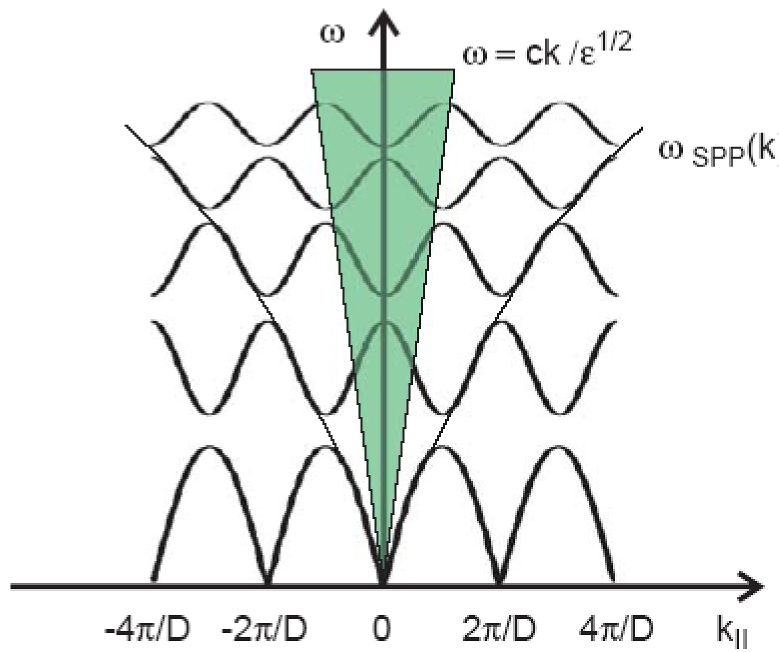

$$k_{sp} = k_x \pm nG_x \pm mG_y \quad G_x = G_y = 2\pi/a_0$$

Ebbesen Group's work

Extraordinary transmission though subwavelength hole array

T. W. Ebbesen *et al.*, Nature (London) **391**, 667 (1998); H. F. Ghaemi *et al.*, Phys. Rev. B **58**, 6779 (1998); T. J Kim *et al.*, Opt. Lett. **24**, 256 (1999); D. E. Grupp *et al.*, Adv. Mater. **11**, 860 (1999).

Experiments

L. Martín-Moreno, et al, PRL 86 1114 (2001)

Theory

Beaming light from a subwavelength aperture

H J Lezec; et al, *Science,* 297 (5582) , 820 (2002)

Hole array + aperture, Hole array + molecular, SPP guiding

PRL 90, 167401 (2003)
PRL 90, 213901 (2003)

PRL 92,107401(2004)

PRB 71,035424 (2005)

PRL 95,046802(2005)

Review Article
Nature 424,824 (2003)

Extraordinary optical transmission through sub-wavelength hole arrays

Bottleneck: low light transmittivity of apertures smaller than the wavelength of incident photon

Hole arrays in silver film:
metal film thickness t
Periodicity of holes a0
Scale of holes d

Results:
Extraordinary transmission
Maximum at $\lambda/d\sim10$
Influence of t (in APL)

Explanation:
Coupling of light and plasmons

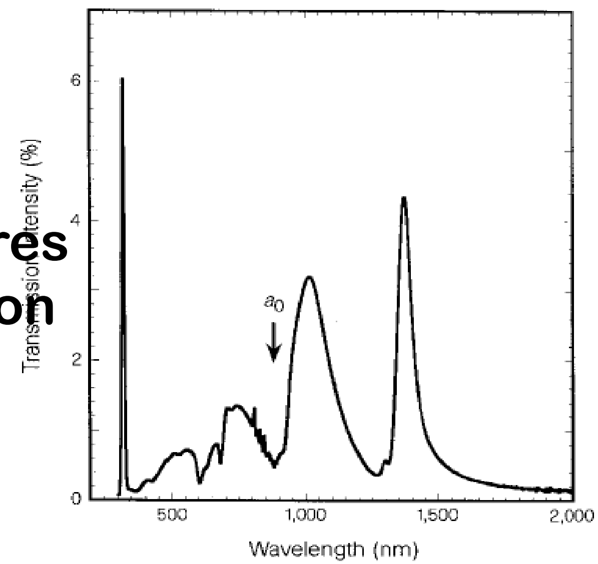

Figure 1 Zero-order transmission spectrum of an Ag array ($a_0 = 0.9\,\mu m$, $d = 150\,nm$, $t = 200\,nm$).

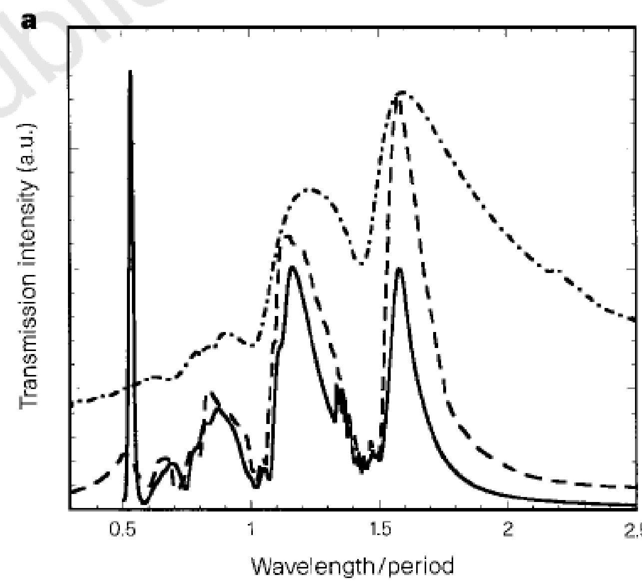

T. W. Ebbesen, H. J. Lezec, H. F. Ghaemi, T. Thio, and P. A. Wolff, Nature (London) **391**, 667 (1998).

Dispersion relations

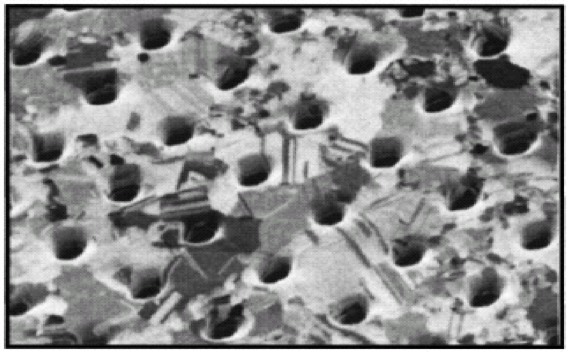

FIG. 1. Focused ion beam image of a two-dimensional hole array in a polycrystalline silver film, with film thickness $t = 200$ nm, hole diameter $d = 150$ nm, and period $a_0 = 900$ nm.

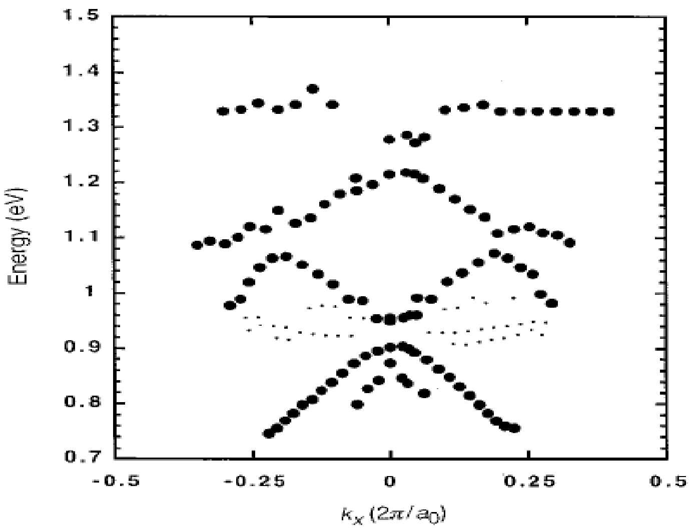

Box 3

Surface plasmon bandgaps

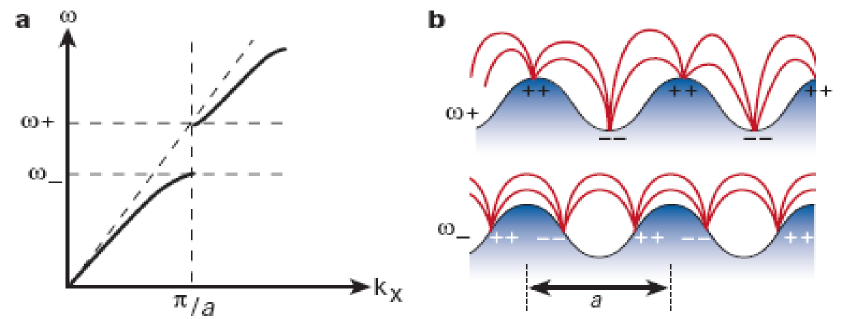

Periodic texturing of the metal surface can lead to the formation of an SP photonic bandgap when the period, *a*, is equal to half the wavelength of the SP, as shown in the dispersion diagram (**a**). Just as for electron waves in crystalline solids, there are two SP standing wave solutions, each with the same wavelength but, owing to their different field and surface charge distributions, they are of different frequencies. The upper frequency solution, ω_+, is of higher energy because of the greater distance between the surface charges and the greater distortion of the field, as shown schematically in **b**. SP modes with frequencies between the two band edges, ω_+ and ω_-, cannot propagate, and so this frequency interval is known as a stop gap. By providing periodic texture in two dimensions, SP propagation in all in-plane directions can be blocked, leading to the full bandgap for SPs. At the band edges the density of SP states is high, and there is a significant increase in the associated field enhancement.

Review Article
Nature 424,824 (2003)

Theory of Extraordinary Optical transmission

surface impedance boundary condition $\lambda \geq L \gg d.$

Theory agrees experiments well, parameters are reasonable

Enhanced transmission is due to tunneling through surface plasmons.

For small thickness h, the photon then goes back and forth several times inside the hole, building up coherent constructive interference in the forward direction much as would occur in electron resonant tunneling.

For larger h, the photon can make fewer round-trips inside the hole before being radiated to infinity, and the concept of plasmon molecule becomes less well defined.

For even larger h, the process is more like sequential tunneling, where the incoming photon gets trapped in a SP, tunnels to the SP at the other interface, and then couples to the outgoing radiative mode and exits.

L. Martý n-Moreno *et al.*, Phys. Rev. Lett. **86**, 1114 (2001).

Effects of hole depth on light transmission

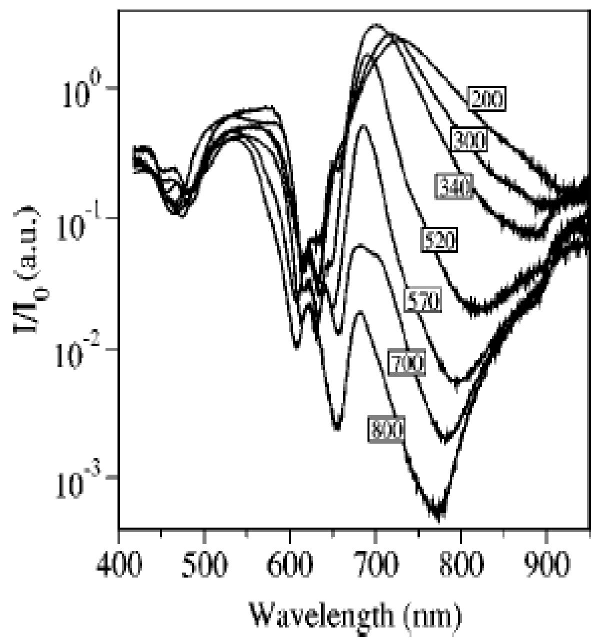

FIG. 1. Zero-order transmission spectra at normal incidence for square arrays of cylindrical holes ($d=300$ nm, $P=600$ nm) for a range of hole depths h, as indicated on each curve.

$$I(h,\lambda_p,d) \propto \exp\left[-\frac{4\pi h}{\lambda_p}\sqrt{\left(\frac{\lambda_p}{1.7d}\right)^2 - 1}\right].$$

For shallow holes, two SPs modes couple as the resonant passage of light through the array.
For deeper holes, the uncoupled SP modes therefore transmission falls exponentially as the film gets thicker.

APL 81,4327(02,ebbesen)

Beaming light from a subwavelength aperture

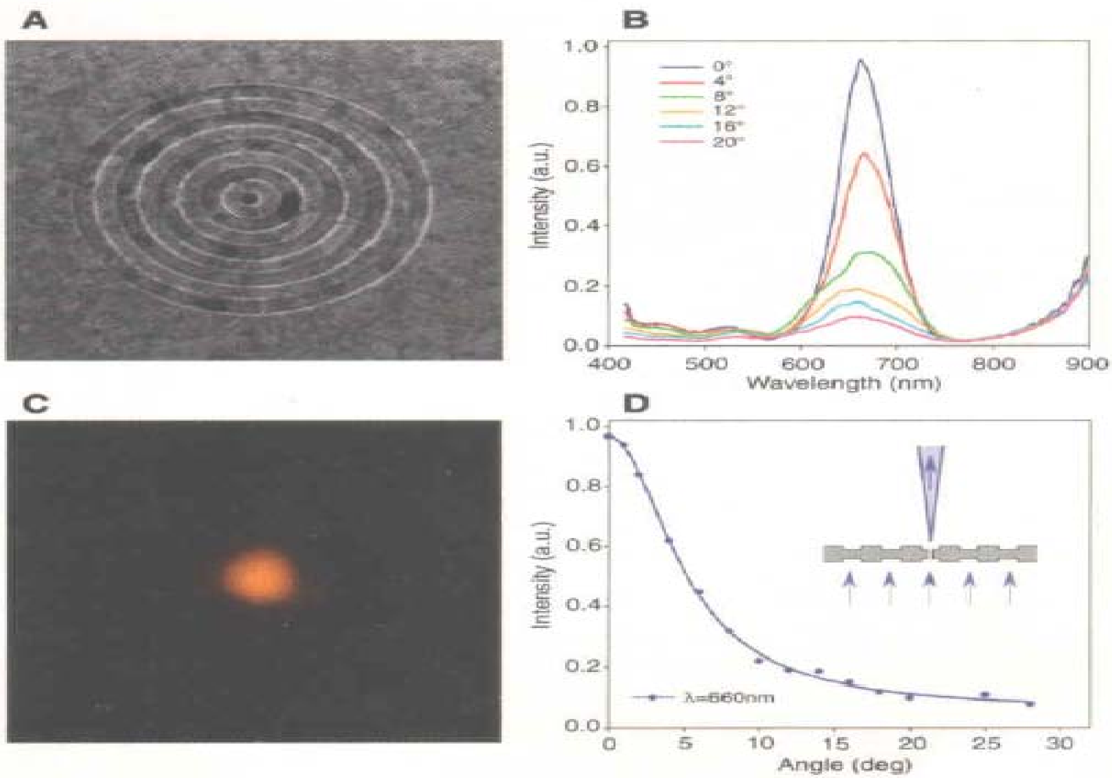

Fig. 1. (**A**) FIB micrograph image of a bull's eye structure surrounding a cylindrical hole in a suspended Ag film (groove periodicity, 500 nm; groove depth, 60 nm; hole diameter, 250 nm; film thickness, 300 nm). (**B**) Transmission spectra recorded at various collection angles for a bull's eye structure on both sides of a suspended Ag film (groove periodicity, 600 nm; groove depth, 60 nm; hole diameter, 300nm; film thickness, 300 nm). The tail above 800 nm is an artifact of the spectral measurement. The structure is illuminated at normal incidence with unpolarized collimated light. The spectra were measured using a Nikon TE200 microscope coupled to an Acton monochromator and a Princeton Instruments CCD (charge-coupled device) camera. (**C**) Optical image of the sample of (A) illuminated from the back at its wavelength of peak transmission (λ_{max} = 660 nm) using a 50-nm band-pass filter. (**D**) Angular transmission-intensity distribution derived from the spectra of (B) at λ_{max}. (Inset) Schematic diagram of the structure and the beam divergence and directionality of the transmitted light at λ_{max} in the far field.

Science 297,820 (2002,ebbesen)

Highly Directional Emission from a Single Subwavelength Aperture Surrounded by Surface Corrugations

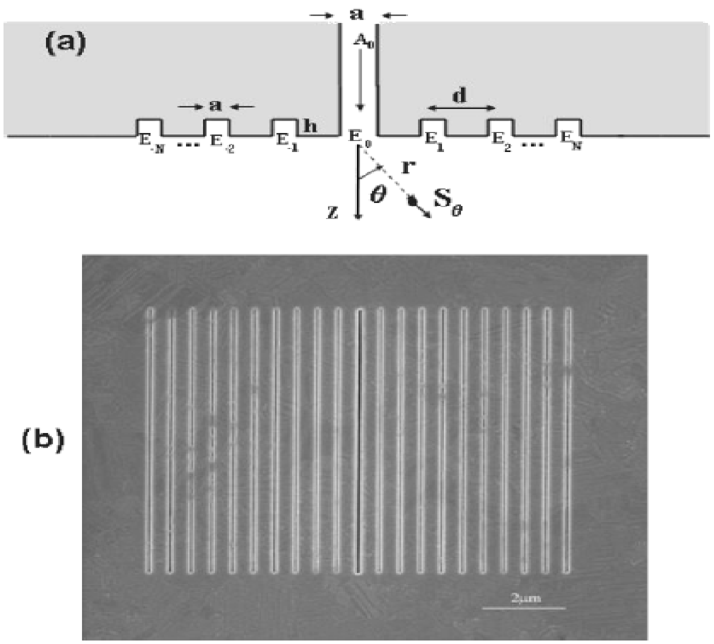

FIG. 1. (a) Schematic picture for the system analyzed: single slit surrounded in the exit surface by a finite array of grooves. In this paper all indentations have width a, and grooves have depth h. (b) Focused-ion-beam image of the exit surface of a slit in a Ag film, with $N = 10$ grooves at each side, and nominal values $a = 40$ nm, $d = 500$ nm, and $h = 100$ nm.

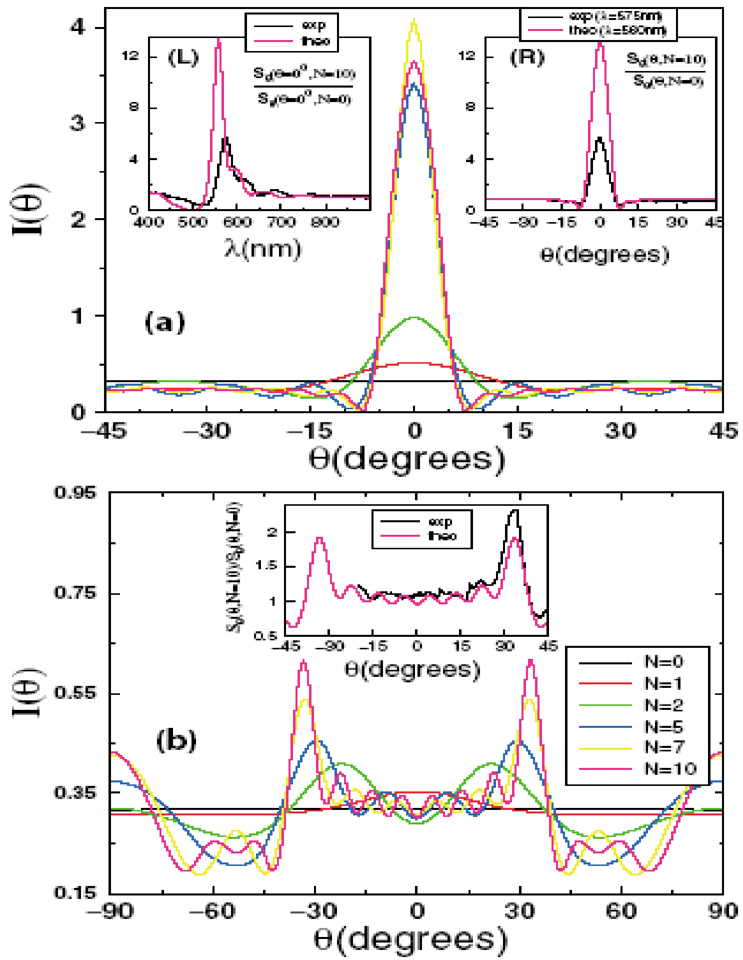

FIG. 2 (color). Calculated angular transmission distribution, $I_N(\theta)$, for $\pm N$ grooves surrounding a central slit. Geometrical parameters as in Fig. 1(b). (a) $\lambda = 560$ nm; (b) $\lambda = 800$ nm. Insets show the comparison between measured and calculated $\Delta S(\theta) = S_\theta(\theta, N = 10)/S_\theta(\theta, N = 0)$. (L): $\Delta S(0)$ vs λ. (R): $\Delta S(\theta)$ at maximum forward beaming ($\lambda^{theo} = 560$ nm, $\lambda^{exp} = 575$ nm). Inset to (b): $\Delta S(\theta)$ for $\lambda = 800$ nm.

PRL 90, 167401 (2003,ebbesen)
PRL 90, 213901 (2003)(subwavelength slit)

Role of SPP in subwavelength hole arrrys

Transmittance maxima are associated with both reflectance minima and absorption maxima

(i) Incident light couples to an SPP mode supported by the surface facing the incident light. The enhanced field associated with an SPP mode increases the probability of transmission through the holes, where it is again scattered by the periodic array to produce light. (ii) Incident light cannot couple to an SPP mode on the incident side, instead matching conditions allow light that is weakly transmitted through the array to couple to an SPP mode on the far side; the enhanced electric field associated with the SPP mode increases the probability of transmission, and subsequent scattering again results in transmitted light. (iii) Matching conditions allow processes (i) and (ii) to take place simultaneously.

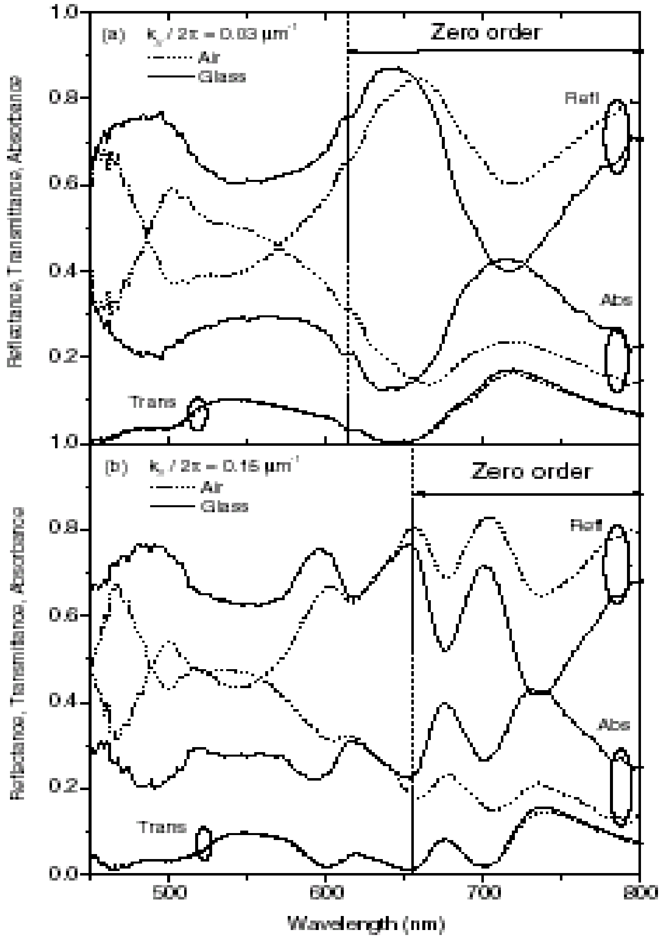

FIG. 4. Transmittance, reflectance, and inferred absorbance spectra for p-polarized incident light at in-plane wave vectors of 0.03 μm^{-1} (a) and 0.15 μm^{-1} (b).

PRL 92,107401(04,ebbesen)

Sambles Group's work

Full Photonic Band Gap for Surface Modes in the Visible

PRL 77,2670(96) 94 experiment
PRB 54 6227(96) 96 theory and a good review

Influence of depth of grating on band gaps

PRL 79, 3978 (97)
PRL 80, 5667 (98)
PRB 65,125415(02) theory and experiment

Extraodinary transmission in microwave region

APL 77,2789 (00)
PRL 89,063901 (02)
APL 84,849 (04)

Other works

Full Photonic Band Gap for Surface Modes in the Visible

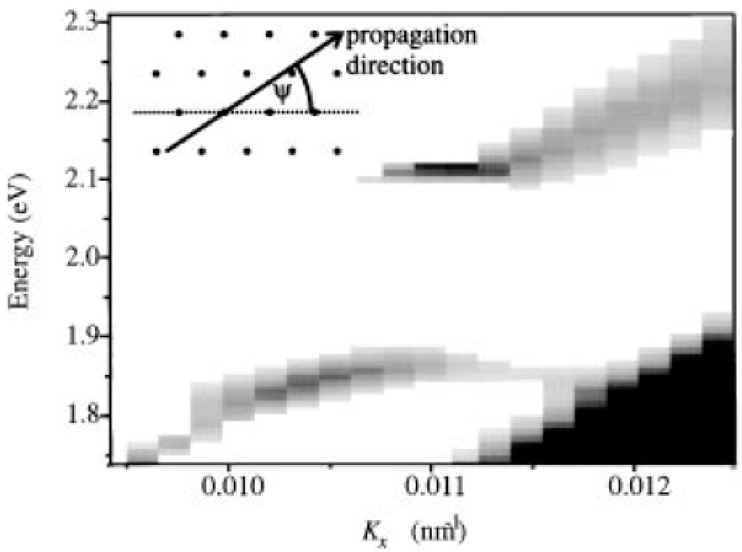

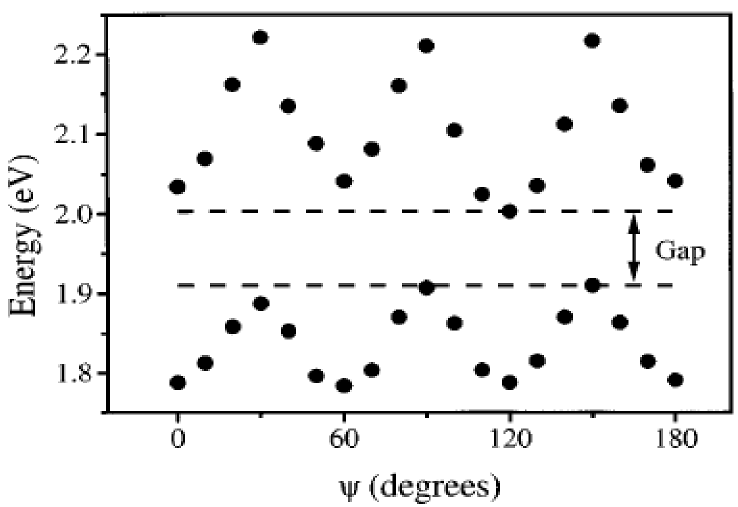

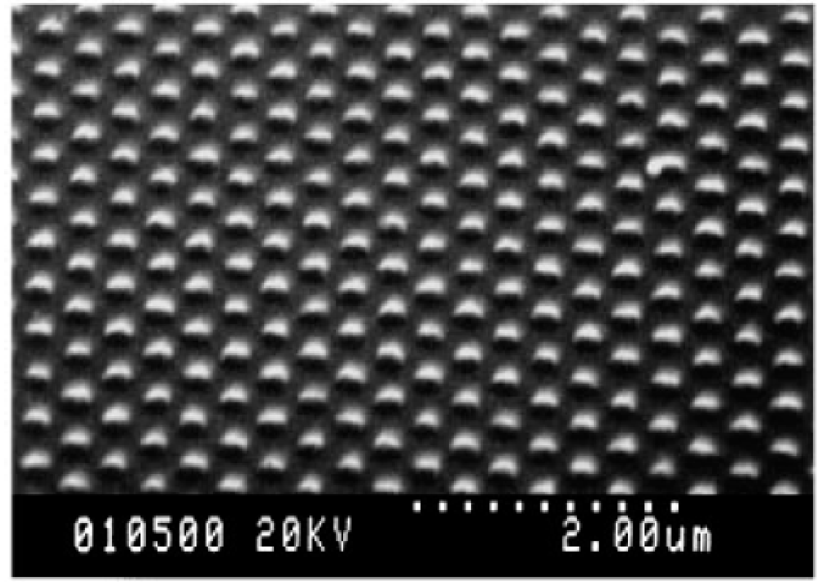

FIG. 1. A scanning electron micrograph of the hexagonal array of dots. The dots are composed of photoresist on a glass substrate. The surface has been coated with a thin film of silver to support the propagation of SPPs.

Period 300nm
Dot radius 100nm
Silver film 40nm

Sambles JR, PRL 77,2670(96)

Other several works

Transition from localized surface plasmon resonance to extended surface plasmon-polariton as metallic nanoparticles merge to form a periodic hole array

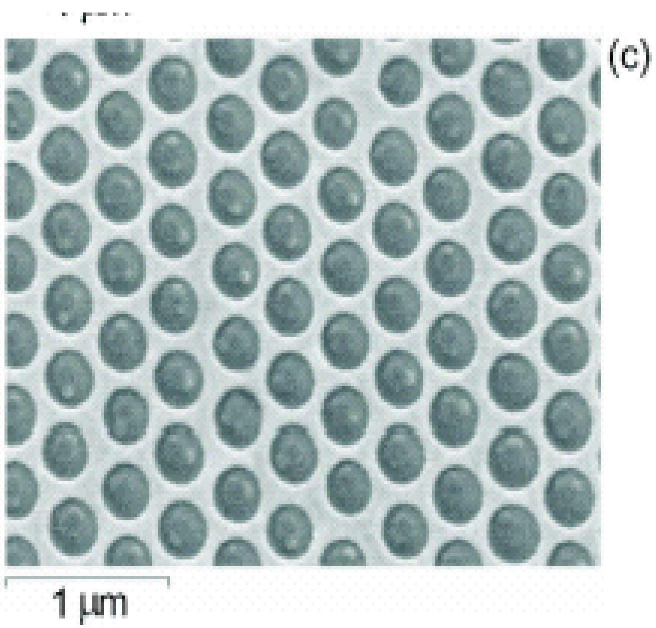

Main results

For individual metallic nanoparticals, Localized SPPs dominate.

For adjacent metallic nanoparticals, A small gap appears.

For a continues metallic thin films, Extended SPPs dominate.

PRB 69,165407(04,barnes)

Transmission of Light through a Single Rectangular Hole

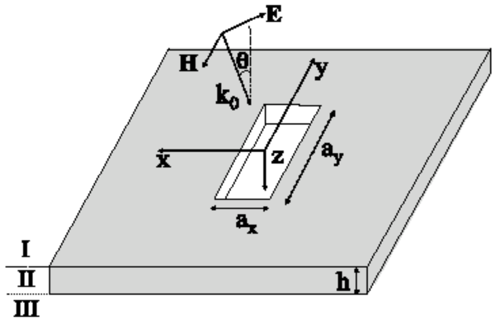

FIG. 1. Diagram of a single rectangular hole of sides a_x and a_y perforated on a metal film of thickness h. The structure is illuminated by a p-polarized plane wave with its angle of incidence with respect to the normal being θ.

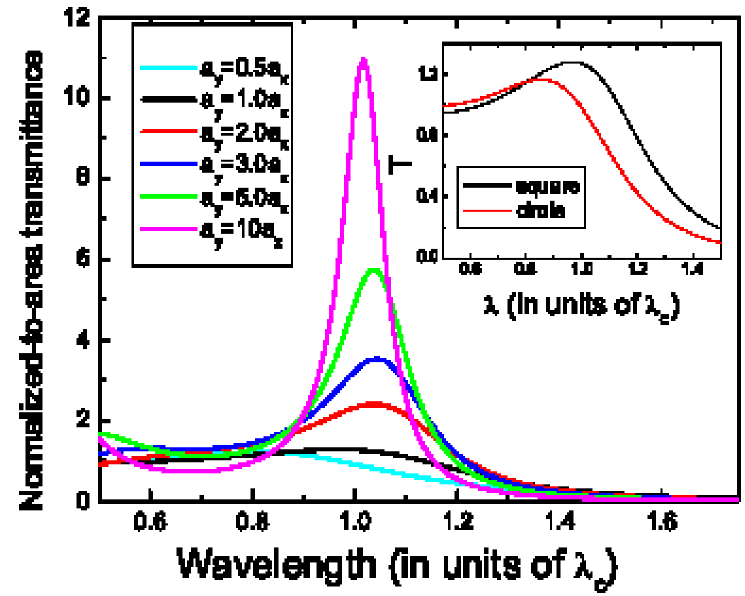

FIG. 2 (color online). Normalized-to-area transmittance (T) versus wavelength (in units of the cutoff wavelength, $\lambda_c = 2a_y$), for a normal incident plane wave impinging on a rectangular hole, for different ratios a_y/a_x. Metal thickness is $h = a_y/3$. For comparison, the inset shows T versus wavelength for a single square (black line) and circular (red line) holes.

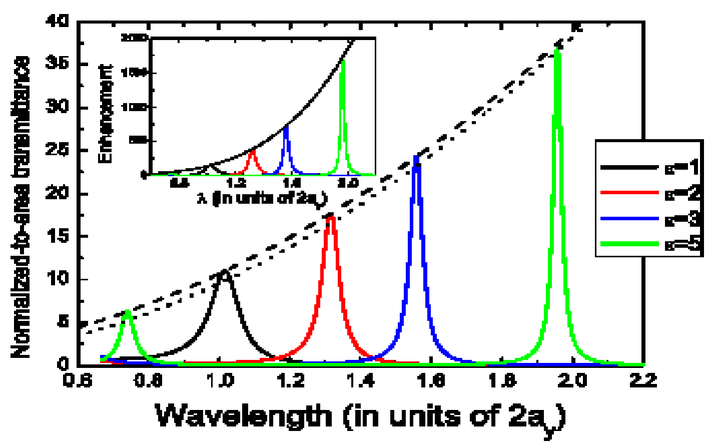

FIG. 3 (color online). T for a normal incident plane wave versus wavelength for a rectangular hole with $a_y/a_x = 10$ and different values of ϵ inside the hole. Metal thickness is $h = a_y/3$. Dashed and dotted lines show the behavior of Eqs. (5) and (6), respectively. Inset: enhancement of the E-field intensity obtained for the previous cases; black curve renders Eq. (7).

Theory

PRL 95,103901(05, F. J. Garcia-Vidal)

纳米金椭球链中的超窄几何共振

参数：

金颗粒尺寸： $60\times40\times15nm^3$

折射率 n=1.46, 周期 h=519nm

原理：

超窄几何峰的出现是由于近场的衍射效应造成。

极化率： $\alpha^* = \dfrac{1}{1/\alpha - S}$

$$S = \sum_{\text{dipoles}} e^{ikr}\left[\frac{(1-ikr)(3\cos^2\theta - 1)}{r^3} + \frac{k^2\sin^2\theta}{r}\right],$$

$$\sigma_{ext} \propto k\,\mathrm{Im}(\alpha^*)$$

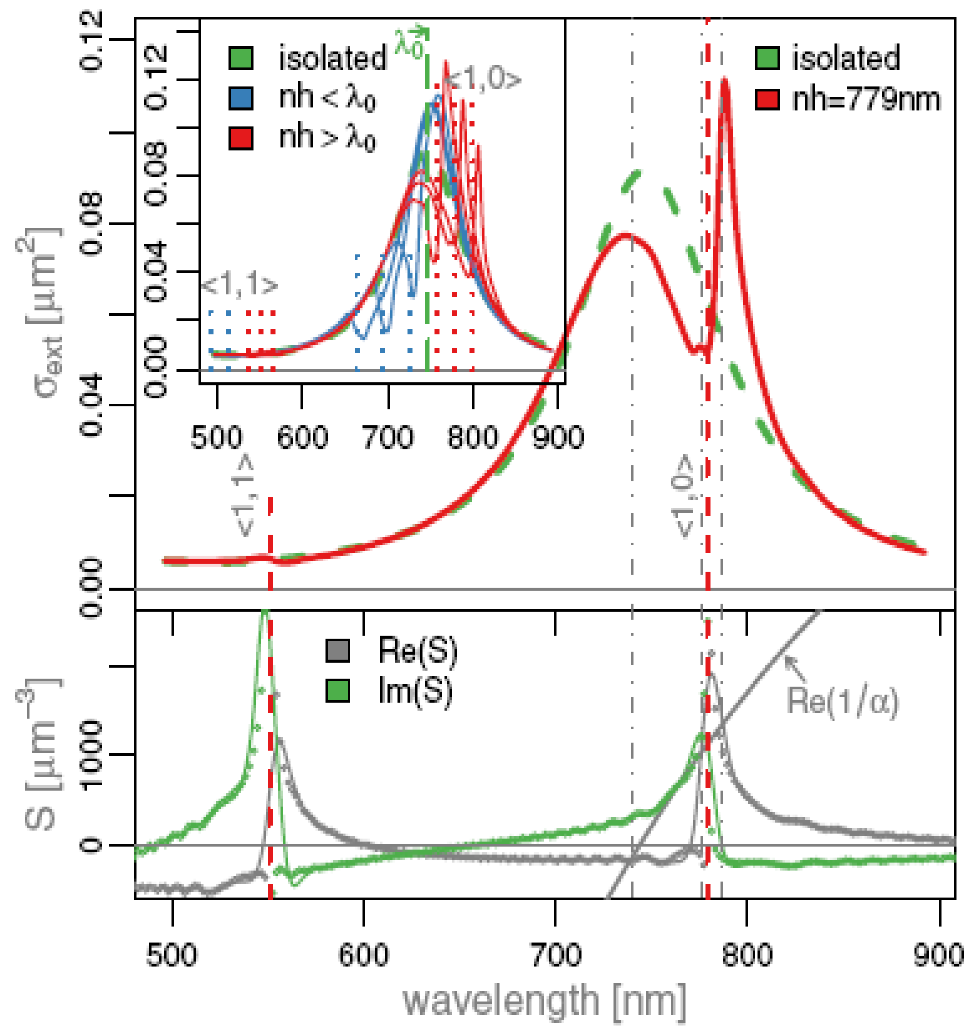

1/α 与S实部的交点导致消光极大。

Collective Resonances in Gold Nanoparticle Arrays，
Baptiste Auguie and William L. Barnes, PRL 101, 143902 (2008)